

# We are IntechOpen, the world's leading publisher of Open Access books Built by scientists, for scientists

4,800

Open access books available

122,000

International authors and editors

135M

Downloads

Our authors are among the

154

Countries delivered to

TOP 1%

most cited scientists

12.2%

Contributors from top 500 universities



WEB OF SCIENCE™

Selection of our books indexed in the Book Citation Index  
in Web of Science™ Core Collection (BKCI)

Interested in publishing with us?  
Contact [book.department@intechopen.com](mailto:book.department@intechopen.com)

Numbers displayed above are based on latest data collected.

For more information visit [www.intechopen.com](http://www.intechopen.com)



# Long-Period Gratings Based on Photonics Crystal Fibers and Their Applications

Chun-Liu Zhao

*Institute of Optoelectronic Technology, China Jiliang University, Hangzhou  
China*

## 1. Introduction

The photonic crystal fiber (PCF) is a special class of components incorporating photonic crystals with a two-dimensional (2D) periodic variation in the plane perpendicular to the fiber axis and an invariant structure along it [1-3]. Typically these fibers incorporate a number of air holes that form a so-called photonic crystal cladding and run along the length of the fibers, and the shape, size, and distribution of the holes can be designed to achieve various novel wave-guiding properties that may not be achieved readily in conventional fibers [2-19], so that they have attracted significant attention in recent ten years.

A long-period fiber grating (LPG) is a one dimension (1D) periodic structure, and is formed by introducing periodic modulation of the refractive index along an optical fiber. Since its period is about 100 to several hundreds  $\mu\text{m}$  and longer than that of fiber Bragg grating (FBG), LPG resonantly couples light from the fundamental core mode to some co-propagating cladding modes and leads to dips in the transmission spectrum. LPGs have been widely used in optical fiber communications and sensors. Examples of LPG-based devices include all-fiber band-rejection filters [20, 21], gain flatteners in erbium-doped fiber amplifiers [22], and sensors for strain, temperature, and external refractive index measurement [23-25]. When a LPG is formed on a PCF, a 2-D periodic structure is combined with a 1-D periodic structure. LPGs based on PCFs (PCF-LPGs) have been fabricated recently [26-36] and shown many unique properties compared with a conventional LPG (1-D periodic structure) [27, 31-34, 37, 38], which provide wide and novel applications [38-47].

In this chapter, we will first introduce the basic operation principle of LPGs, secondly, will demonstrate in detail the strain and temperature characteristics of a LPG based on an endlessly-single-mode (ESM) solid silica core PCF theoretically. To account for the effect of dispersive characteristics of the PCF, we identify a dispersion factor  $\gamma$ , which offers a deeper understanding into the behavior of LPGs in PCF. Following, we will move on to the fabrication of a PCF-LPG by using a  $\text{CO}_2$  laser and demonstrate the experimental observations on the strain and temperature characteristics, which agree with the theoretical predictions very well. Finally, we will demonstrate their applications in optical sensors, including a temperature-insensitive strain sensor, and demodulation technologies for fiber Bragg grating and fiber loop mirror sensors.

## 2. Basic operation principle of LPGs [23, 38, 48]

A LPG is formed usually by a periodic modulation of the refractive index in a fiber core, which allows coupling from the fundamental core mode to some resonant cladding modes and leads to some dips in the transmission spectrum at wavelengths that satisfy the resonant condition. The phase matching condition of a LPG can be expressed as [23]:

$$\lambda = (n_{co} - n_{cl})\Lambda \quad (1)$$

where  $\lambda$  is the resonant wavelength,  $\Lambda$  is the index modulation period of the LPG, and  $n_{co}$  and  $n_{cl}$  are the effective indices of the fundamental core mode, and the forward-propagating cladding mode, respectively.

When an axial strain is applied on the LPG, the resonant wavelength of the LPG will shift because the  $\Lambda$  of the LPG will increase with stretching axially and at the same time the effective refractive index of both core and cladding modes will decrease due to the photo-elastic effect of the fiber [31]. Meanwhile, if the ambient temperature changes, the wavelength of the LPG may also be changed by linear expansion or contraction and the thermo-optic effect. From equation (1), the sensitivity of the LPG to strain or temperature is a function of the differential effective index between the core and cladding modes (or the differential propagation constant). Thus, from equation (1), the strain and temperature sensitivity can be written as [48]:

$$\frac{d\lambda}{d\varepsilon} = \lambda \cdot \gamma \cdot \left(1 + \frac{\eta_{co}n_{co} - \eta_{cl}n_{cl}}{n_{co} - n_{cl}}\right) \quad (2)$$

$$\frac{d\lambda}{dT} = \lambda \cdot \gamma \cdot \left(\alpha + \frac{\xi_{co}n_{co} - \xi_{cl}n_{cl}}{n_{co} - n_{cl}}\right) \quad (3)$$

where  $\varepsilon$  is the axial strain,  $T$  is the ambient temperature,  $\eta_{co}$  and  $\eta_{cl}$  are strain-optic coefficients of the core and cladding,  $\xi_{co}$  and  $\xi_{cl}$  are the thermo-optic coefficient of the core and cladding, respectively, and  $\alpha$  is the linear expansion coefficient.  $\eta$  and  $\xi$  are defined as [23]:

$$\eta = \frac{1}{n} \frac{dn}{d\varepsilon} \quad (4)$$

$$\xi = \frac{1}{n} \frac{dn}{dT} \quad (5)$$

Different materials have different  $\eta$  and  $\xi$ .  $\eta$  and  $\xi$  may also have some difference due to the different effective index of waveguides made by the same material [49].

Since the effective index (or propagation constant) both of the fundamental mode in the fiber core and cladding modes in the fiber cladding will be affected by the waveguide change which is caused by the applied axial strain on the LPG, the dispersion factor  $\gamma$  is used to describe the effect of waveguide dispersion and is expressed as [48]:

$$\gamma = \frac{d\lambda/d\Lambda}{n_{co} - n_{cl}} = \frac{\Delta n_e}{\Delta n_e - \lambda \frac{d\Delta n_e}{d\lambda}} = \frac{\Delta n_e}{\Delta n_g} \quad (6)$$

where  $\Delta n_e = n_{co} - n_{cl}$  and  $\Delta n_g = n_{co}^g - n_{cl}^g$  are respectively the differential effective index and differential group index between the core mode and the cladding mode. As will be discussed in Section 3,  $\gamma$  plays a significant role on the strain and temperature sensitivity of an LPG based on the PCF.

### 3. Theoretical properties of an LPG based on PCF [38]

In this section, we investigate in detail the strain and temperature characteristics of an LPG based on an endlessly single-mode (ESM) solid silica core PCF theoretically. To account for the effect of dispersive characteristics of the PCF, we identify a dispersion factor, which offers a deeper understanding into the behavior of PCF-LPGs. Theoretical results show that is always negative, and this causes blue-shifting of the resonant wavelength when an axial strain is applied.

#### 3.1 Properties of the ESM-PCF

The PCF used in the work is an endlessly single-mode PCF fabricated by Crystal Fiber A/S. The fiber has a standard triangular air/silica cladding structure, as shown in Fig. 1 (a). The mode field diameter is  $\sim 6.4 \mu\text{m}$ , the center-to-center distance between the air holes ( $L$ ) is  $\sim 7.78 \mu\text{m}$ , and the diameter of the air holes is  $\sim 3.55 \mu\text{m}$ . The diameter of the entire holey region is  $\sim 60 \mu\text{m}$ , and the outer cladding diameter of the PCF is  $125 \mu\text{m}$ . A full-vector finite-element method (FEM) was used to calculate the effective index of modes of PCF. Because of the symmetric nature of the PCF, only a quarter of the cross-section as shown in Fig.1 (b) is used during calculation. A perfect electric or perfect magnetic conductor (PEC or PMC) was applied at boundaries [7]. The refractive index of pure silica was taken as 1.444.

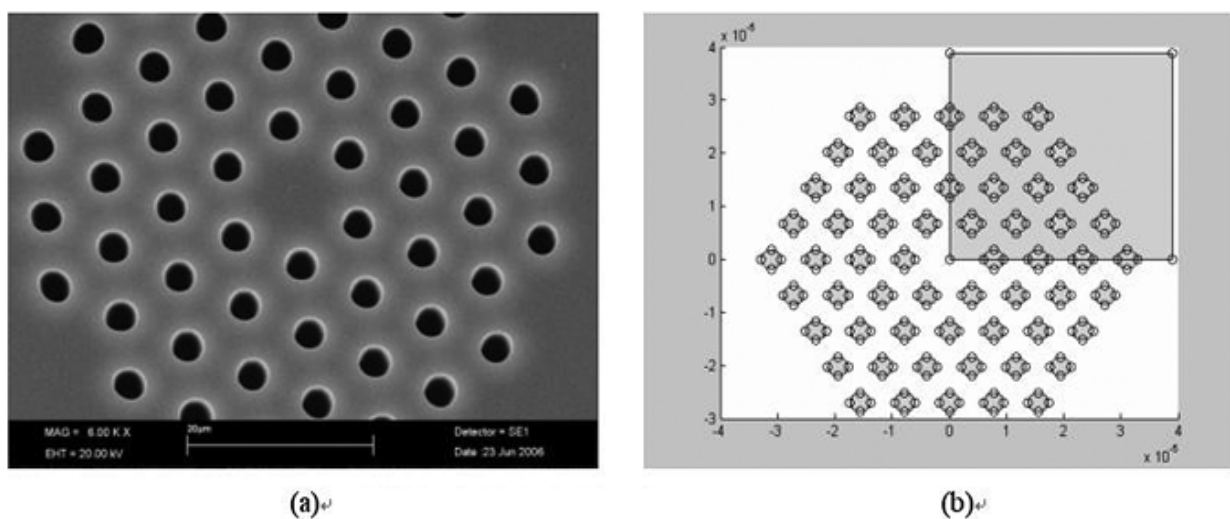


Fig. 1. (a) Micrograph of the PCF used in the experiment; (b) Schematic cross-section of a PCF, showing the quarter used in calculation

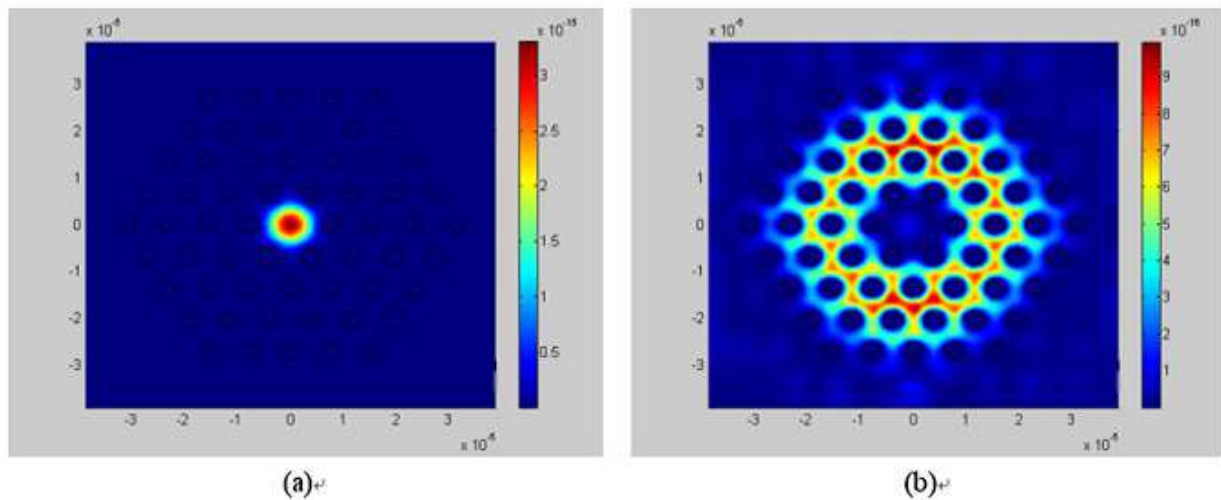


Fig. 2. Calculated intensity distribution of the PCF with  $L=7.78 \mu\text{m}$  and  $d=3.55 \mu\text{m}$ . (a) The fundamental core mode; (b) The cladding mode

Fig. 2 (a) and (b) shows the intensity distribution of the core and the cladding mode, which are considered as the two coupling modes in our PCF-LPGs. Fig. 3 shows the effective indices of the fundamental and cladding modes as functions of wavelength in the ESM-PCF.

The group indices of these two modes, which were calculated by using  $n_g = n_e - \lambda \frac{dn_e}{d\lambda}$ , are also shown in Fig. 3. The curves of  $n_g$  are not so smooth because of the limited data available for the calculation of  $\frac{dn_e}{d\lambda}$  but the trend is clear. The curve  $n_{g-cl}$  shows the highly dispersive characteristics of the cladding mode. For any wavelength in the range of  $1.2 \sim 1.8 \mu\text{m}$ , the group index of the cladding mode is higher than that of the core mode, which is in contrast to a conventional SMF.

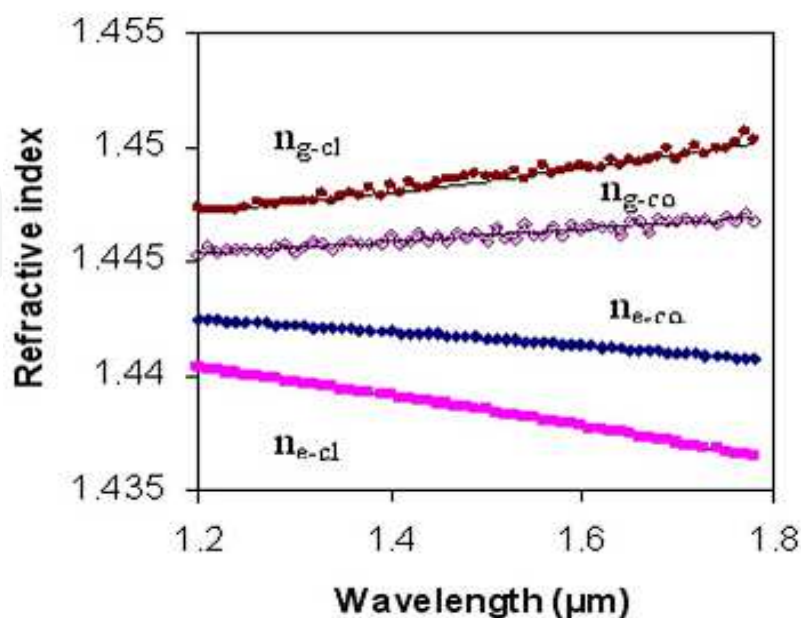


Fig. 3. Calculated dispersion curves for core and cladding modes as shown in Fig. 2.

### 3.2 Properties of an LPG based on the PCF in theory

Fig. 4 shows the calculated resonance wavelength as a function of the period of PCF-LPG. It is clear that the resonance wavelength of PCF-LPG decreases with increasing LPG period, which is consistent with other experimental observations [27, 33, 34]. This is in contrast to LPGs written in conventional SMFs and is because of the highly dispersive property of the cladding mode due to the existence of the air-holes. In other words,  $(n_{co} - n_{cl})$  as shown in equation (1), varies significantly with wavelength.

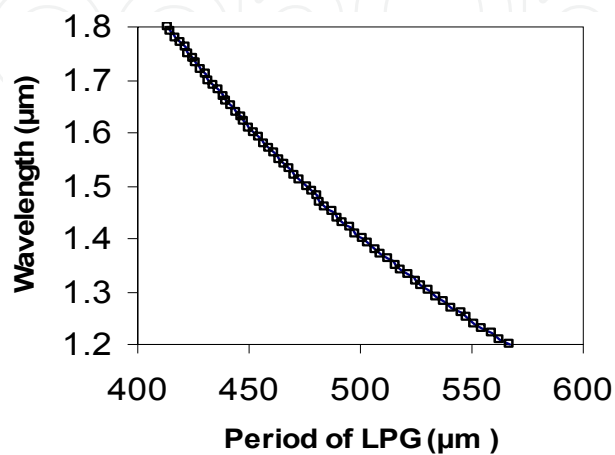


Fig. 4. Calculated resonance wavelength as a function of grating period

$\gamma$  is a special factor to describe the effect of waveguide dispersion, and  $\gamma$  may be positive or negative. Because  $\Delta n_e$  is always positive, the sign of  $\gamma$  is determined by  $\Delta n_g$ . When  $\Delta n_e$  equals to  $\Delta n_g$ , the factor  $\gamma$  is 1. This means dispersive properties of the core and the cladding mode is similar and this is the case normally for SMFs. When the group indices of the core mode is less than that of the cladding mode,  $\gamma$  will be negative. This has been observed in the case of the coupling from core mode to higher-order cladding modes in B-Ge co-doped fiber [48]. In Fig. 5, we show the relationship of  $\gamma$  with the period of a LPG based on the theory of ESM-PCF, and  $\gamma$  is in the range of -1.15~ -1.35 for LPG period of from 420 to 570μm.

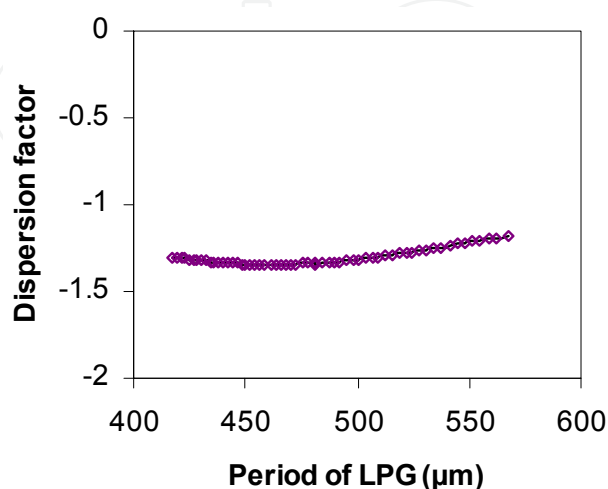


Fig. 5. Dispersion factor  $\gamma$  at the resonance wavelengths vs. grating period of the PCF-LPG

The strain sensitivity  $d\lambda/d\varepsilon$  of a LPG based on the ESM-PCF is determined by four parameters: the elasto-optic coefficients of the core and cladding materials, waveguide properties ( $\gamma$ ), the period of the LPG, and the mode order. Now, we choose the same coupling modes, and focus on the effect of the first three parameters on the strain sensitivity of a PCF-LPG. Fig. 6 shows the calculated strain sensitivity as a function of LPG period with different  $\eta_{cl}$  when we assume  $\gamma = 1$ . In the calculation,  $\eta_{co}$  is assumed to be constant at a value of -0.22 for the pure silica core. For LPGs with period ranging from 400 to 600  $\mu\text{m}$ , the strain sensitivity is positive and relatively independent of the grating period when  $|\eta_{cl}|$  is larger than 0.22. The strain sensitivity becomes negative and decreases with grating period when  $|\eta_{cl}|$  is smaller than 0.218. On the other hand, when the value of  $\gamma$  is taken the value as shown in Fig. 5, the strain sensitivity as a function of LPG period is as shown in Fig. 7. The strain sensitivity is negative when  $|\eta_{cl}|$  is larger than 0.22. This is the opposite of what is shown in Fig. 6. In ref. [49], A. Bertholds et. al. showed that the strain-optic coefficients of a bulk silica and a silica fiber are different. It's believed that, owing to the different geometry of solid core and micro-structured air-silica cladding of the ESM-PCF,  $\eta_{co}$  will be slightly different from  $\eta_{cl}$ .

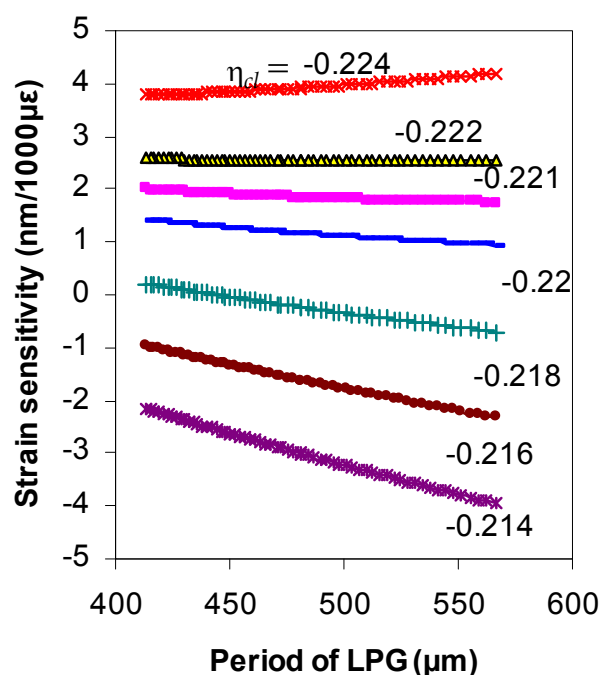


Fig. 6. Theoretical strain sensitivity at resonance wavelength vs. LPG period for various values of  $\eta_{cl}$  and  $\gamma = 1$ .

Similarly, the temperature sensitivity  $d\lambda/dT$  of a LPG is determined by the thermo-optic coefficients of the core and cladding materials, waveguide properties ( $\gamma$ ), period of LPG, and the mode order. We calculated the temperature sensitivity as a function of LPG period by assuming that the thermo-optic coefficient of the pure silica core is  $\xi_{co} = 7.8 \times 10^{-6} / ^\circ\text{C}$  and thermal expansion coefficient is  $\alpha = 4.1 \times 10^{-7} / ^\circ\text{C}$ . Figs. 8 and 9 show respectively the results for the cases of  $\gamma = 1$  and  $\gamma$  taking from Fig.5. The temperature characteristics are quite different for the two cases. With  $\xi_{cl}$  less than  $\xi_{co} = 7.8 \times 10^{-6}$ , the LPG has positive temperature sensitivity for  $\gamma = 1$  but negative temperature sensitivity for the case of  $\gamma$  taking from Fig.5.

Furthermore, the dependence of temperature sensitivity on the grating period is approximately linear for  $\gamma = 1$  while it is non-monotonic for the other case. Similar to the discussion for the strain coefficient, for the ESM-PCF, since the effective index  $n_{co}$  is larger than  $n_{cl}$ , from eq. (5), we expect that  $\xi_{co}$  is slightly smaller than  $\xi_{cl}$ , which has also been verified by the experiment in Section 4.

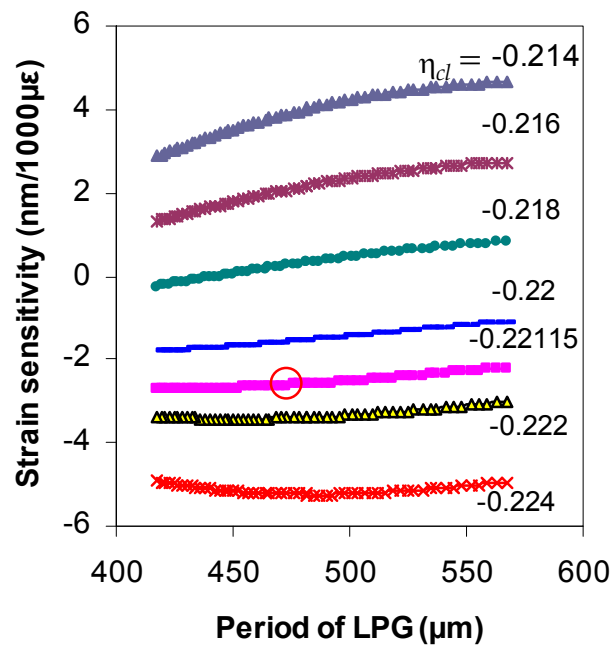


Fig. 7. Theoretical strain sensitivity at resonance wavelength vs. LPG period for various values of  $\eta_{cl}$  and with  $\gamma$  taken from Fig. 5.

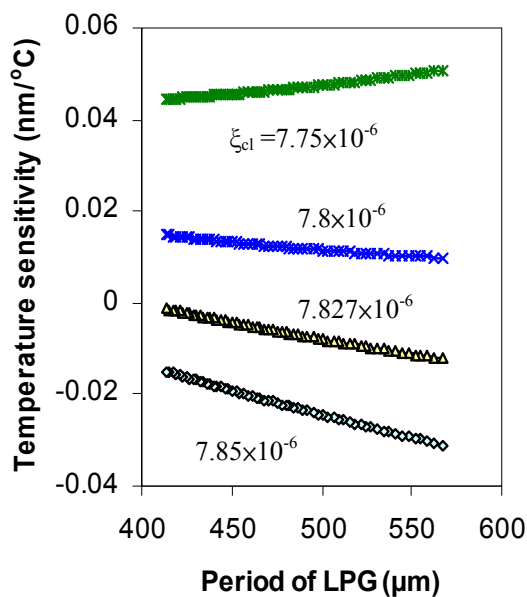


Fig. 8. Theoretical temperature sensitivity at resonance wavelength vs. LPG period for various values of  $\xi_{cl}$  and  $\gamma = 1$ .



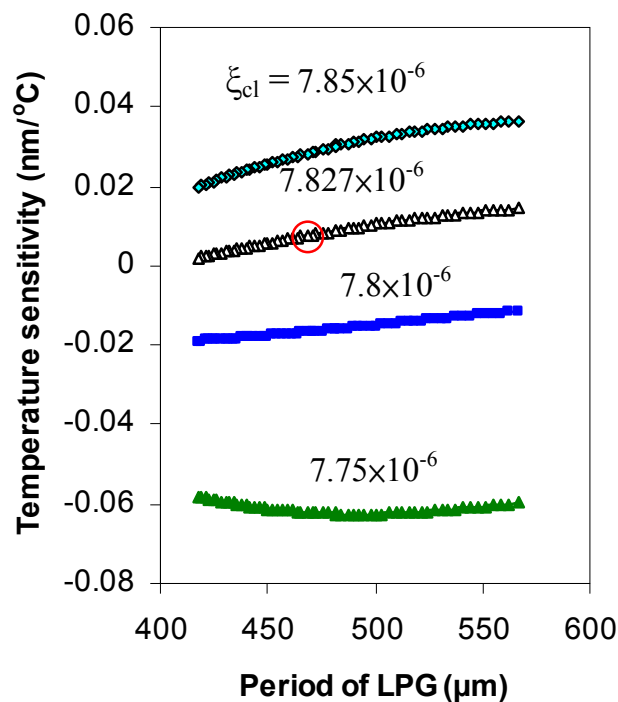


Fig. 9. Theoretical temperature sensitivity at resonance wavelength vs. LPG period for various values of  $\xi_{cl}$  and with  $\gamma$  taken from Fig. 5.

#### 4. Fabrication and experimental observations on properties of a LPG based on PCF [38]

##### 4.1 Fabrication of a PCF-LPG

Unlike conventional fibers, which contain at least two different glasses each with a different thermal expansion coefficient, thereby giving rise to a relatively high thermal expansion coefficient, PCFs are virtually insensitive to temperature because it is made of only one material (and air holes). This property can be utilized to obtain temperature-insensitive PCF-based devices, as demonstrated in [14]. However, the single material property of PCFs leads to non-photosensitivity to UV light, therefore FBGs and LPGs cannot normally be formed in PCFs by use of the conventional UV-written technique, unless a PCF with a Ge-doped photosensitive core is used [26]. Recently, several alternative methods for making LPGs in PCFs with non-photosensitive cores were introduced, including glass structure change [27], periodic structural and/ or residual stress relaxation induced by arc discharge or a CO<sub>2</sub> laser [28-32], refractive index modulation by periodically applied mechanical pressure [33] or by the use of an acoustic wave [34, 35], and periodic drilling micro-holes with a femto-second laser [36].

LPGs fabricated by use of a CO<sub>2</sub> laser are compact and stable because the perturbations are everlasting whereas in LPGs fabricated by UV light in conventional fibers, the refractive index modulation caused by UV light are prone to aging, therefore making LPGs in conventional fibers unstable over time. Here, we demonstrate the fabrication method by using a CO<sub>2</sub> laser, which has been used widely [30, 32, 37, 38, 40].

Fig. 10 shows the experimental setup of the PCF-LPG fabrication. The CO<sub>2</sub> laser operates at a frequency of 10 kHz and has a maximum power of 10 W. The laser power is controlled by the width of the laser pulses. In the experiment, the pulse-width of the CO<sub>2</sub> laser was chosen to be 3.8  $\mu$ s. The laser beam was focused to a spot with a diameter of  $\sim$ 60  $\mu$ m and scanned across the ESM-PCF transversely and longitudinally along the fiber by use of a two-dimensional optical scanner attached to the laser head. The scanning step of the focused beam was 1  $\mu$ m and the delay time of each step was 350  $\mu$ s. The LPG inscribed has a period of about 467  $\mu$ m and a period number of 40. The process of the CO<sub>2</sub> laser scanning is repeated 9 times, which results in a LPG with a deep transmission dip and no observable deformity in the fiber structure. The spectrum measurements were performed using a broadband light source (a light-emitting diode, LED, with the wavelength range of 1200  $\sim$ 1700 nm) in combination with an optical spectrum analyzer (OSA, ADVANTEST Q8384) with a resolution of 0.5 nm.

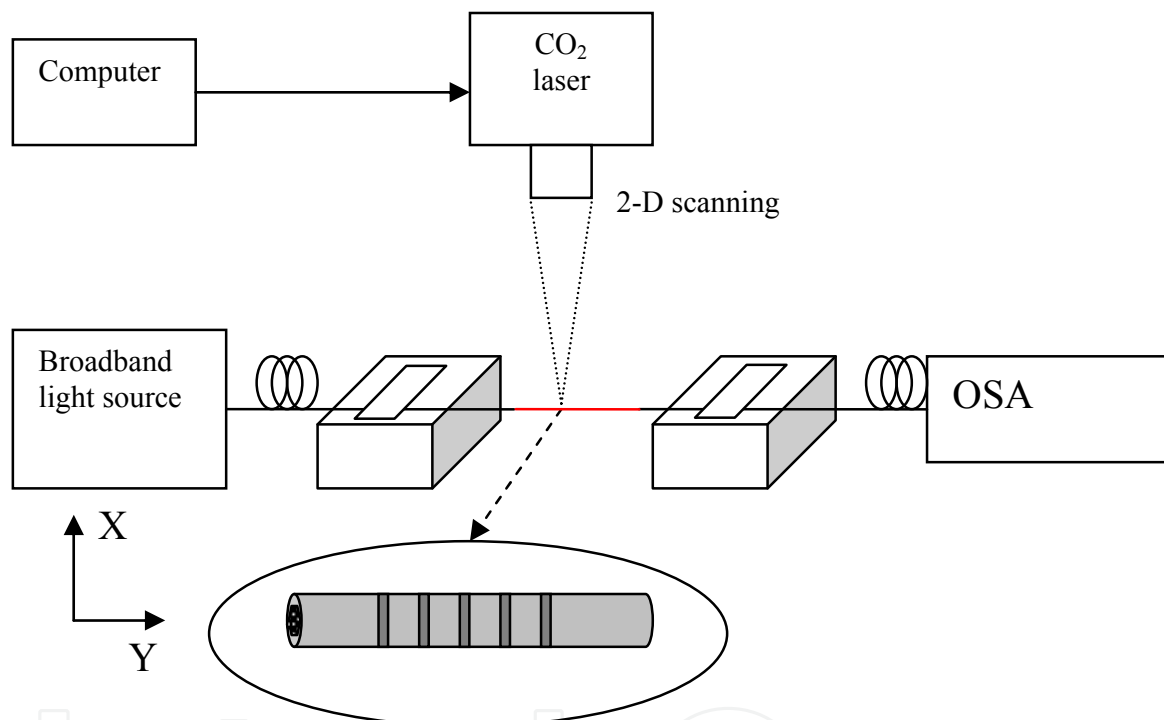


Fig. 10. Schematic of the PCF-LPG fabrication setup

Fig. 11 shows the growing process of a PCF-LPG as a function of the number of scanning procedures. The resonant wavelengths of the PCF-LPG are about 1552.45 nm and 1363.3 nm which are due to coupling of the fundamental core mode to two different cladding modes. The dip at the wavelength 1552.45 nm is nearly 20 dB. The insertion loss of the LPG is about 1.5 dB. The resonance at 1552.45 nm is due to coupling of the core mode to the cladding mode shown in Fig. 2 (b) and is in good agreement with the theoretical result (1552.45 nm resonance wavelength corresponds 467.2  $\mu$ m LPG period) in Fig. 4.

#### 4.2 Properties of a LPG based on PCF in experiment

Fig. 12 shows the experimental setup for measuring the characteristics of the PCF-LPG. The spectrum measurements were performed by using a broadband LED and an OSA with a

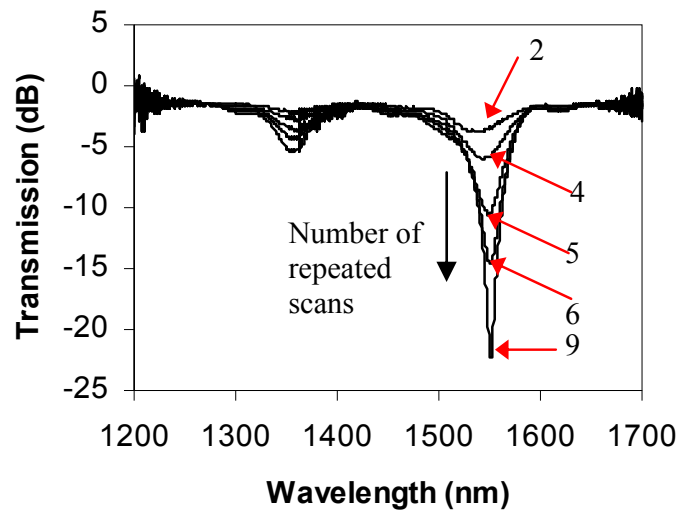


Fig. 11. Transmission spectra of the PCF-LPG with various numbers of repeated scans

resolution of 0.5 nm as mentioned in Section 4.1. The strain characteristics of the PCF-LPG was tested by stretching the PCF-LPG by moving the translation stage shown in Fig. 10 from 0 to 0.5 mm in four steps (corresponding to a strain variation of from 0 to 1604  $\mu\epsilon$ ), the center wavelength of the transmission dip shifts toward shorter wavelength as shown in Fig. 13. This is opposite to a LPG in a conventional SMF where the transmission dip shifts toward longer wavelengths [23]. The strain dependence of the resonance wavelength 1552.45 nm on axial strain is shown in Fig. 14. The strain sensitivity, which is the slope of the curve, is estimated to be -2.68 nm/ 1000  $\mu\epsilon$  and shown in Fig.7 as a small circle. By varying the strain coefficient of the cladding material  $\eta_{cl}$  to fit the experimental data, we found the value of  $\eta_{cl}$  that best fits the experimental sensitivity is  $\eta_{cl} = -0.22115$ . The transmitted intensity at resonance wavelength was found increases with the applied axial strain, and this is also shown in Fig. 14.

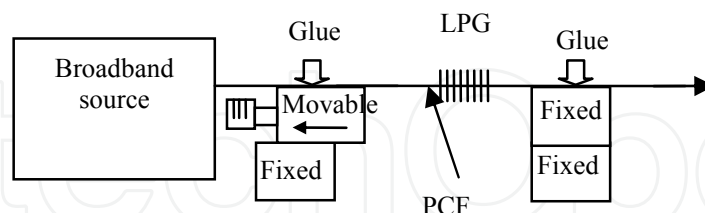


Fig. 12. Experimental setup for measuring the temperature and strain characteristics of the PCF-LPG, where a broadband source and an OSA are used.

To test the temperature characteristics of the PCF-LPG, the ambient temperature of the LPG was varied by using a temperature chamber whose temperature can be controlled within the range of 25 °C to 100 °C. As shown in Fig.15, the transmission spectrum hardly changes when temperature was raised from 25 °C to 100 °C. The estimated sensitivity of the resonant wavelength to temperature is about 0.007 nm/ °C. Again, the temperature sensitivity of the PCF-LPG is marked as a circle in Fig.9. The cladding temperature coefficient  $\xi_{cl}$  that fits this

temperature insensitivity is  $\xi_{cl} = 7.827 \times 10^{-6}$ , this value is slightly larger than that of the core and agrees with the prediction at the end of Section 4.2. It should be noted that the difference between  $\xi_{co}$  and  $\xi_{cl}$  for the PCF is 6 times smaller than that of conventional Ge-doped fiber and 18 times smaller than that of B-Ge co-doped fiber [48].

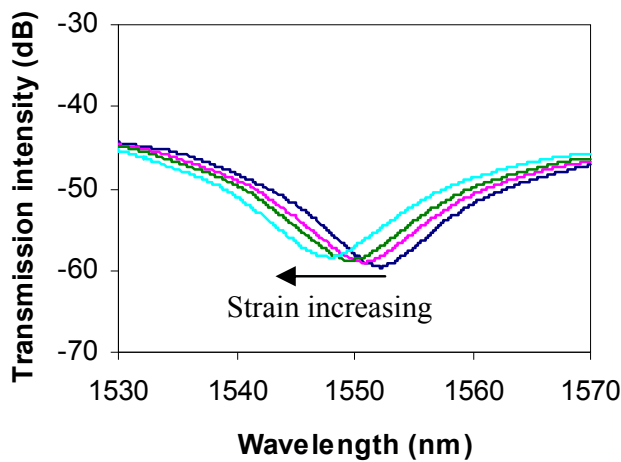


Fig. 13. Transmission spectra of the PCF-LPG for applied strain of (from right to left) 0, 535, 936, and 1604  $\mu\text{m}$

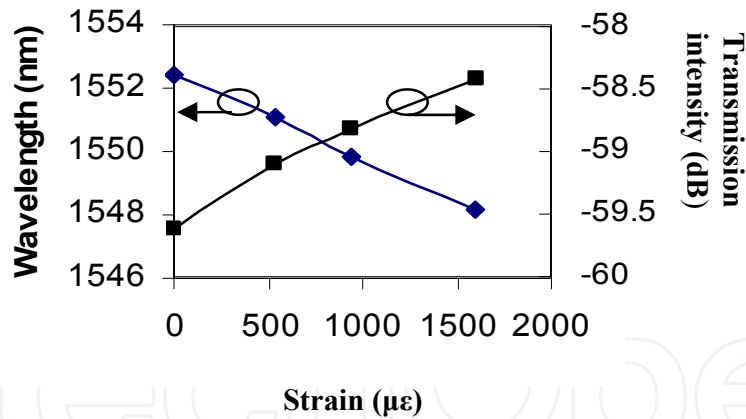


Fig. 14. Resonant wavelength and the intensity at the transmission dip as functions of applied strain

## 5. Applications of an LPG in PCF in optical fiber sensors

### 5.1 Temperature-insensitive strain sensor based on a PCF-LPG [38]

By exploiting the PCF-LPG’s large sensitivity to strain and insensitivity to temperature, temperature-insensitive strain sensors are realized. These sensors can be based on either wavelength or intensity measurement. In this part, we demonstrate a simple, low cost strain sensor based on the measurement of the transmitted light intensity at a wavelength close to the LPG resonance.

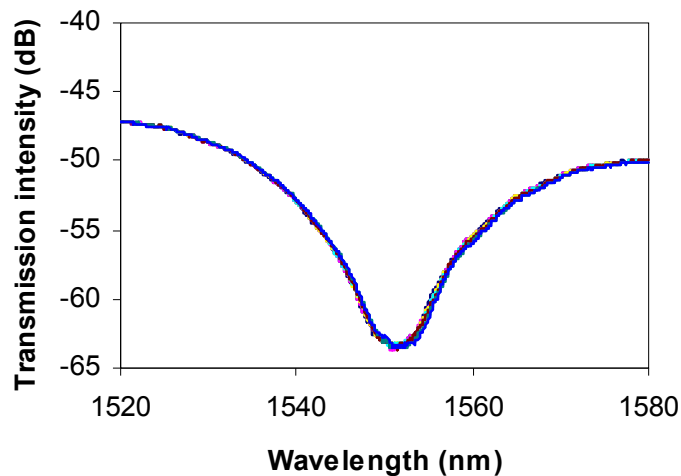


Fig. 15. Transmission spectra of the LPG in the ESM PCF at various ambient temperatures

Fig. 16 shows the proposed strain sensor that uses the PCF-LPG as the sensing element. A single wavelength light such as a DFB laser is used as a light source. The wavelength of the DFB laser is near the resonant wavelength of the LPG and hence the output light intensity from the LPG will be directly related to the LPG's transmission at the wavelength of the DFB laser. Since the LPG's transmission is insensitive to temperature, the output power will only be affected by the transmission spectrum change caused by the strain applied to the LPG. At the output, an optical power meter will be adequate to deduce the strain information and an expensive OSA would not be needed.

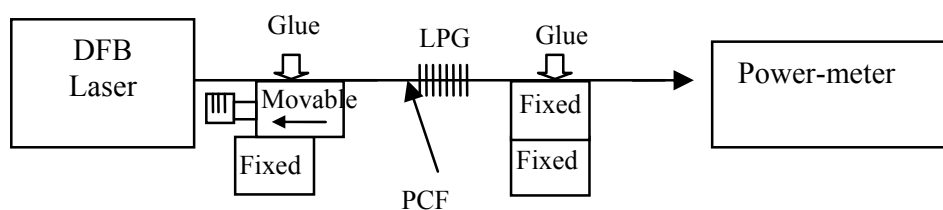


Fig. 16. The proposed temperature insensitive strain sensor with a DFB laser and an optical power meter

Fig. 17 shows the measured relationship between the output intensity of the PCF-LPG sensor and the applied axial strain for various laser wavelengths. In the experiment, a tunable laser was used for easiness of wavelength adjustment. In practice, a DFB laser with appropriate wavelength would be a better for the purpose of reducing cost. As shown in Fig.17, for laser wavelengths of 1538 nm, 1542 nm, 1545 nm, and 1547.7 nm, which are shorter than the resonant wavelength (1552.45 nm) the LPG, the output intensity decreases with applied strain and the strain sensitivity is negative and respectively -1.41, -2.17, -2.80 and -2.41 dB/1000  $\mu\epsilon$  for 1538 nm, 1542 nm, 1545 nm, and 1547.7 nm. The relationship is approximately linear for strains from 0 to 1600  $\mu\epsilon$ . Similarly, for laser wavelength longer than the resonant wavelength (1552.45nm), the output intensity increases with applied strain and the intensity sensitivities are positive and respectively 3.25, 3.11, 2.01 and 1.53 dB/ 1000  $\mu\epsilon$  at 1553 nm, 1555.6 nm, 1560

nm, and 1563 nm. Therefore, the setup shown in Fig. 16 converts directly the strain variation to intensity variation. Assume that we choose a DFB laser at 1553nm as source, and use an optical power meter with a resolution of 0.001 dB, we may achieve a strain resolution of  $\sim 0.3\mu\epsilon$ .

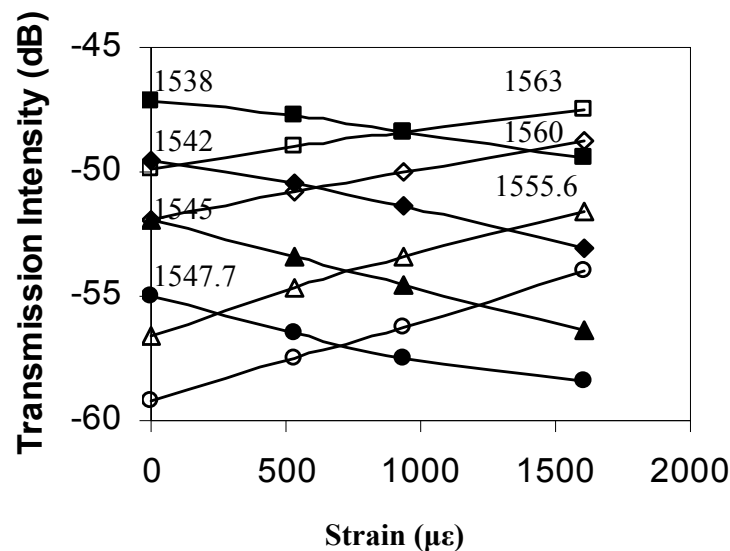


Fig. 17. Strain dependence of the transmission intensity of the PCF-LPG at different wavelengths

## 5.2 Temperature-insensitive demodulator based on a PCF-LPG for a fiber Bragg grating temperature sensor [45]

Fiber Bragg grating (FBG) is another kind of optical fiber grating, and is formed by a periodic modulation of the refractive index along an optical fiber with  $\sim 0.5 \mu\text{m}$  pitch  $\Lambda$ , which causes the coupling between the forward-propagating core mode to the backward-propagating core mode at the reflective wavelength satisfied with the phase matching condition  $\lambda_B = 2n_{eff}\Lambda$ , where  $\lambda_B$  is the reflective wavelength,  $n_{eff}$  is the effective refractive index of the core mode, respectively. By fabricating FBG with different pitch, we can get different reflective wavelength of FBG. The bandwidth of FBG is narrow compared with that of LPG, because the coupling strength decreases rapidly when the wavelength departs from  $\lambda_B$ . FBGs have been applied widely in sensors. Because of the wavelength-encoded nature of the FBG sensors, it is necessary to convert the wavelength-encoded signal into electronic signals for easy reading and real time monitoring.

In this part, we present the use of PCF-LPG for the purpose of making a temperature insensitive sensor interrogation based on the PCF-LPG's much lower temperature sensitivity and realize a whole fiber Bragg grating (FBG) temperature sensor, including a sensor head and a PCF-LPG readout component, in one package. Utilizing the wavelength-dependent transmission loss of the LPG, the wavelength change of the FBG due to the temperature of the environment is translated to the intensity of the output. At the output, only a power meter is required to deduce the temperature of the environment and an expensive OSA would not be needed. The experimental results show that the interrogation based on the PCF-LPG works well under different environmental temperatures.

Fig. 18 shows the schematic diagram and the experimental setup of the proposed fiber Bragg grating temperature sensor interrogation system using an LPG in a PCF. The sensor head was made of a FBG and was illuminated using a broadband LED via a 3-ports circulator. The sensor head was placed inside a temperature-controlled container in order to detect its sensitivity to temperature. The reflected light from the sensor head is returned to the circulator and enters the PCF-LPG. In the experiment, the central reflection wavelength of the FBG sensor head was chosen as shown in Fig. 19. The FBG was fabricated in a hydrogen-loaded single-mode fiber using a phase mask illuminated by UV light. The phase mask had a constant period of 1068 nm (the corresponding grating period is 534 nm). The original centre wavelength of the FBG sensor is at 1546.3 nm, which is located at the middle of the wavelength range of the transmission spectrum of the LPG with the negative slope. The reflected light from the sensor head is transmitted partially by the PCF-LPG and the amount of transmission is a function of wavelength. The wavelength shift of the FBG sensor head with temperature is almost linearly related to the transmission function of PCF-LPG filter for the range of operation. The power at the output of the PCF-LPG is directly related to the temperature applied on the FBG because as the temperature increases, the wavelength of the light reflected by the FBG shifts more to a longer wavelength, which in tune causes the light to leading to PCF-LPG to decrease in intensity. At the output, only a power meter is enough to deduce the temperature of environment. Thus it is very feasible to monitor the variation in temperature by measuring the output power of the PCF-LPG in a relatively cheap manner.

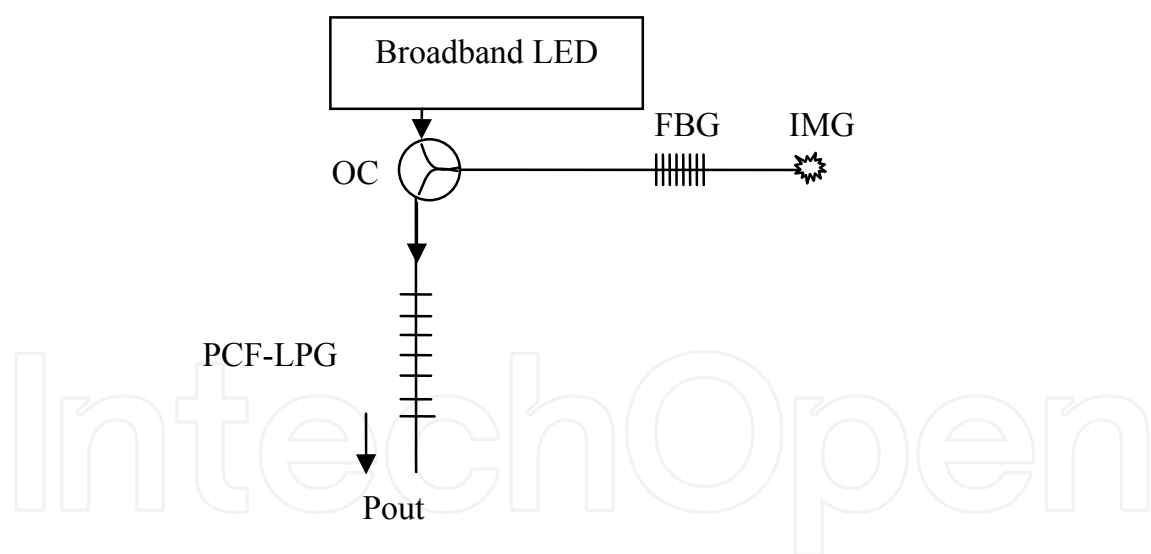


Fig. 18. Schematic diagram of the proposed temperature sensor interrogation system based on a PCF-LPG, IMG: index matched glue, OC: optical circulator.

When the FBG sensor was put into a temperature chamber and the temperature was increased from 25 to 100 °C, the Bragg reflection of the FBG would shift to longer wavelengths due to the thermo-optic effect and the thermo-expansion effect of the optical fiber. Fig. 20 shows the output spectra. The intensity of the output changes in accordance with the transmission curve of the PCF-LPG, which is as the reflection wavelength of the FBG gets longer, the output of the PCF-LPG gets smaller. Fig. 21 shows the relationship of

the output intensity of the PCF-LPG with the temperature on the FBG and that this relationship is virtually linear for temperature from 25 to 100 °C. In this temperature range (75 °C), the change in the reflected wavelength from the FBG is 0.75 nm, and the intensity change of the output power via the LPG is 1.2 dB. Thus the sensitivity of the proposed FBG temperature sensor is about -0.0165 dB/ °C. Because the slope of the transmission spectrum in the wavelength range from 1545 to 1548 nm is virtually constant as implied by Fig. 21, the linear dynamic range of this temperature sensor is at least 300 °C. Therefore, this setup converts the temperature variation to wavelength variation (FBG) and then it converts the wavelength variation to intensity variation (PCF-LPG).

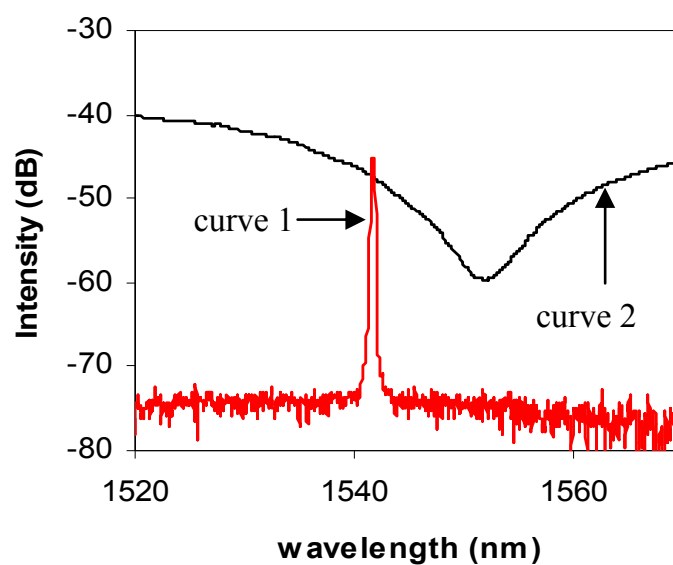


Fig. 19. The reflective spectrum of the FBG (curve 1) at room temperature and the transmission spectrum of the LPG (curve 2)

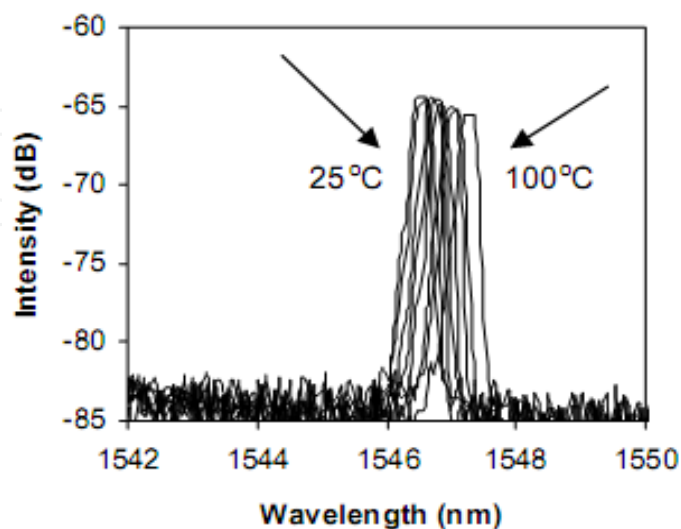


Fig. 20. The output spectra from PCF-LPG when a different temperature (25 °C, 30, 40, 50, 60, 70, 80, 90, 100 °C) is applied to the FBG.



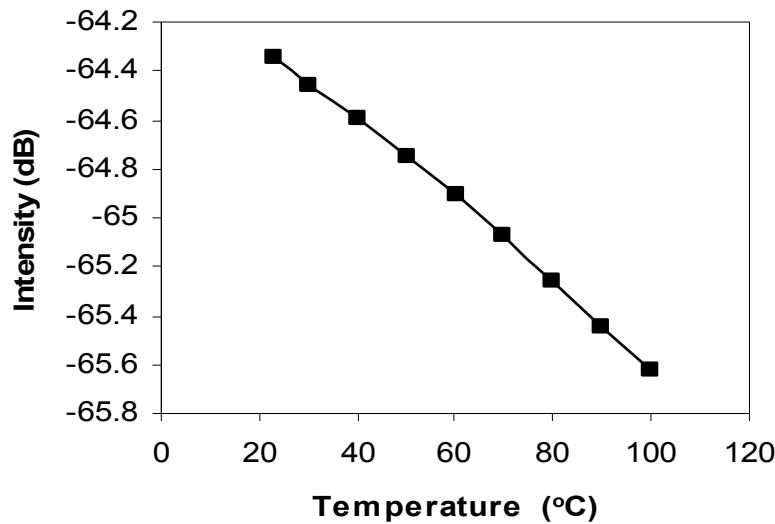


Fig. 21. The measured output power for the temperature of the grating sensor

### 5.3 A fiber loop mirror temperature sensor demodulation technique based on a PCF-LPG and a band-pass filter [46]

Fiber loop mirrors (FLMs) have been demonstrated for a number of applications, for example wavelength filters and sensors [14, 15, 50]. In a FLM, two interfering waves counter-propagate through the same fiber, and are exposed to the same environment. This makes it less sensitive to environmental disturbance. Various kinds of sensors based on FLMs have been realized, such as temperature sensors, strain sensors, pressure sensors, liquid level sensors, biochemical sensors, UV detection, multi-parameter measurement and refractive index sensors. However, most HiBi-FLM sensors are based on monitoring the resonant wavelength variation of FLMs [15, 51], an expensive OSA is needed.

In this part, we present a HiBi-FLM temperature sensor using a PCF-LPG and a band-pass filter as a demodulator. For the sensing principle, only the HiBi-FLM acts as a sensor head, while the PCF-LPG serves as a filter to provide wavelength dependent optical power transmission and the band-pass filter is to provide a narrow band light source. By utilizing the stable filtering function of the PCF-LPG, the resonant wavelength variation of the FLM with temperature is transferred effectively to the intensity variation of the output light. When the optical intensity of the output is monitored, temperature applied on the FLM will be deduced. The experimental results show the demodulator based on the PCF-LPG and the band-pass filter works well. By choosing a filter with an appropriate bandwidth, the temperature sensitivity of the sensor with 1.742 dB/ °C is obtained.

Fig.22 shows the experimental setup. The configuration of the proposed sensor system includes a broadband light source, a band-pass filter, a HiBi-FLM, and a PCF-LPG. A broadband superluminescent LED (SLED) source with a flatten emission intensity in the wavelength range of 1530~1570 nm was used as an input light source, whose power is ~40 mW. The SLED with a band-pass filter launches the HiBi-FLM via a 3 dB coupler. The transmitted light from the HiBi-FLM then enters the temperature-insensitive PCF-LPG. The

proposed sensor demodulation was used to read in optical power and an optical power meter (NF1112) with a resolution of 0.01 dB is used to monitor the output light intensity of the sensor. For monitoring transmission spectra of the FLM and the PCF-LPG, and explaining the principle of the sensor system, an OSA is used in experiments with a spectral resolution of 0.02 nm.

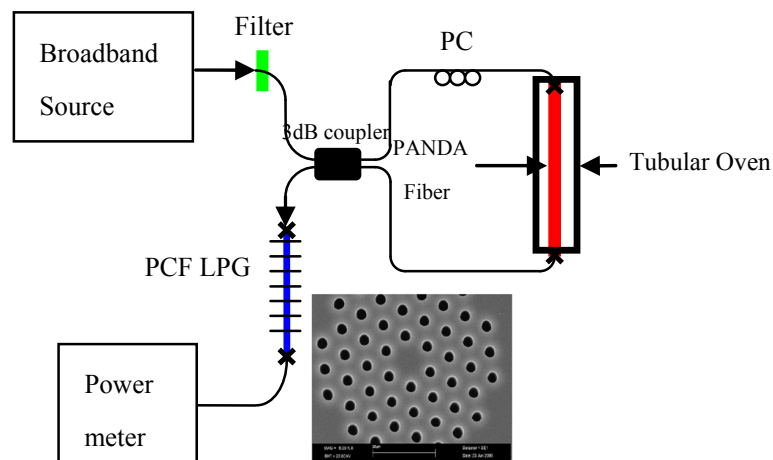


Fig. 22. Experimental setup of the proposed sensor, inset: micrograph of PCF.

The HiBi-FLM includes a 3 dB coupler, a 30.5 cm Panda PMF, and a polarization controller (PC). The Panda PMF has an attenuation of 1.0 dB/km, a measured birefringence of  $\Delta n = 6.24 \times 10^{-4}$  at 1550 nm, and a core diameter  $\sim 10 \mu\text{m}$ . Both ends of the Panda fiber were spliced to Corning SMF-28, and the combined loss of the two splicing points is 2.3 dB. The wavelength spacing between transmission peaks of the FLM is given by  $\Delta\lambda = \lambda^2 / \Delta n \cdot L$ , where  $\lambda$ ,  $\Delta n$ , and  $L$  are wavelength, birefringence and length of the HiBi fiber, respectively. The wavelength spacing between the transmission peaks of the FLM is about 13 nm at 1545 nm, as shown in Fig. 23. In the experiment, this value was chosen by considering the bandwidth of the PCF-LPG. When the PCF-LPG is given, a suitable wavelength spacing of the FLM can be obtained by choosing the length of the PMF. Thus by adjusting the state of the PC, one spectral peak of the FLM is located in a negative of the linear regions with the PCF-LPG at the initial state of the sensor. The temperature-insensitive of the PCF-LPG used in the experiment is the same one as mentioned above.

The band-pass filter is made of Metal-Dielectric-Metal (MDM), which is used to provide a narrow band light source. As shown the gray region in the Fig. 23, only the intensity in the band-pass of the filter is monitored by the optical power meter. In the experiment, several filters with the same center wavelength at 1545nm and different bandwidth are used to study the effect of the bandwidth of the filter on the sensing performance. The full width at half maximum (FWHM) of the band-pass filters is 12.66nm, 8.3 nm, 6.66 nm and 3 nm, respectively, whose transmission spectra are shown in Fig.24.

Fig.25 shows transmission spectra of the PCF-LPG, the HiBi-FLM, and the output signal at different temperature when the band-pass filter is not inserted. When temperature is increased, the transmission spectrum of the FLM blue-shifts due to thermally induced refractive index change and thermal expansion of the panda fiber, and the temperature sensitivity to wavelength is  $-0.772 \text{ nm}/^\circ\text{C}$ . Due to the filtering function of the PCF-LPG, the

intensity of the resonant peak1 increases while the resonant peaks shift to shorter wavelength with temperature increasing. Therefore, when a band-pass filter is used, as shown in Fig.23, the part of the output light outside the band of the filter is attenuated owing to the function of the band-pass filter. And the intensity of the remainder will change with the transmission peak of the HiBi-FLM shifting. Therefore, converting the wavelength variation of the HiBi-FLM into intensity variation at the output directly is realized.

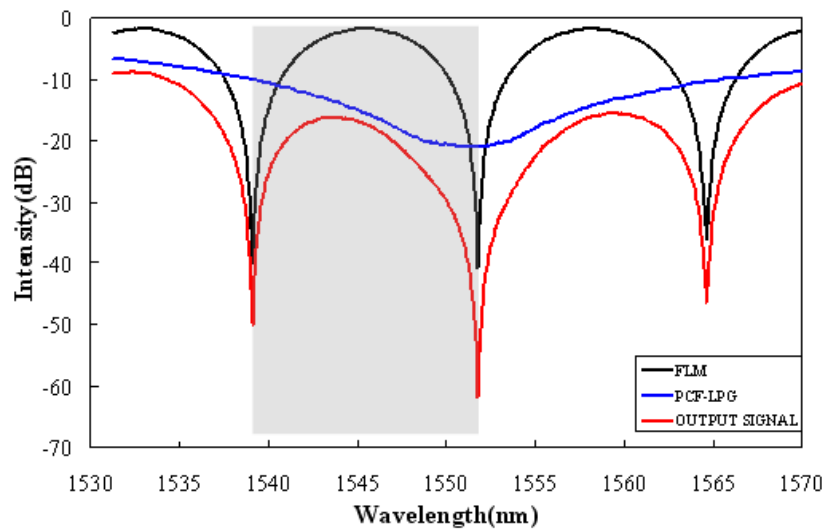


Fig. 23. Transmission spectra of the FLM, the PCF-LPG and the output signal. Gray region is transmission spectra of the sensor with band-pass filter.

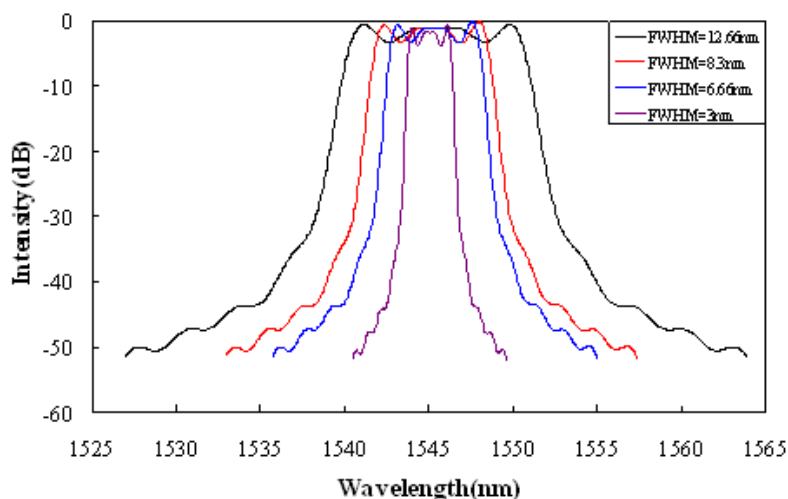


Fig. 24. Transmission spectra of the band-pass filters used in the experiment.

Fig.26 shows the relationship of the output intensity of the sensing system with temperature applied on the FLM, when the filter was chosen with a FWHM 12.66 nm and a center wavelength at 1545 nm. The output intensity is approximately a periodic function of temperature. The period is 16 °C and temperature increases from 45.5 °C to 61.5 °C in a period. This behavior can be explained by the periodic property of the FLM. Since the transmission spectrum of the FLM is approximately a periodic function of the wavelength, the peaks of the FLM enter, then shift outside the pass-band of the filter one by one when

the peaks of the FLM shift to shorter wavelengths with temperature increasing. Therefore, the intensity of the output light changes periodically with temperature increasing. The change in the transmission wavelength of the FLM is 13nm corresponding to 16 °C temperature period, which is consistent with the wavelength spacing of 13 nm between the transmission peaks of the FLM. In order to certify the explaining, we take out the band-pass filter and measure the transmission spectra of the output signal at three different temperatures, which are marked in Fig.26.

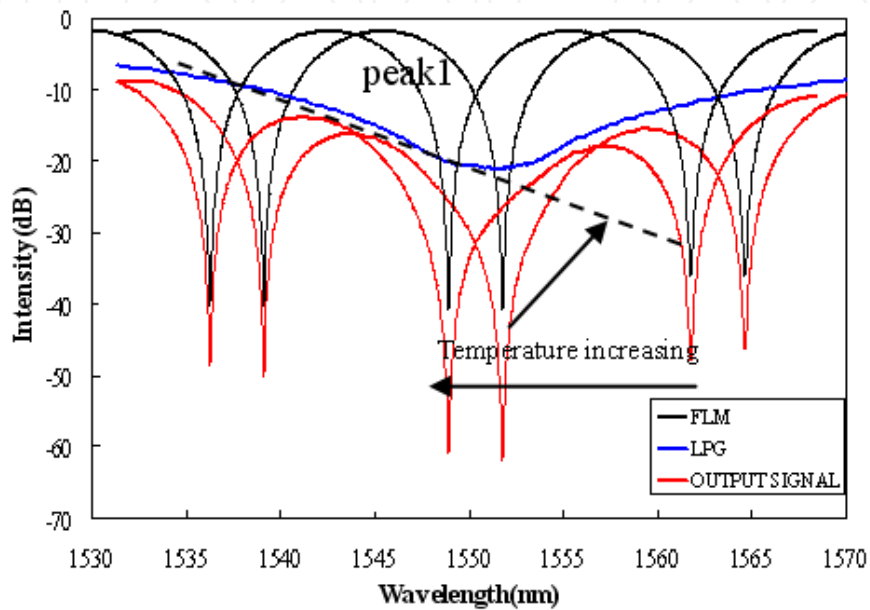


Fig. 25. Transmission spectra of the FLM, the PCF-LPG and output signal when temperature is applied to the sensing head.

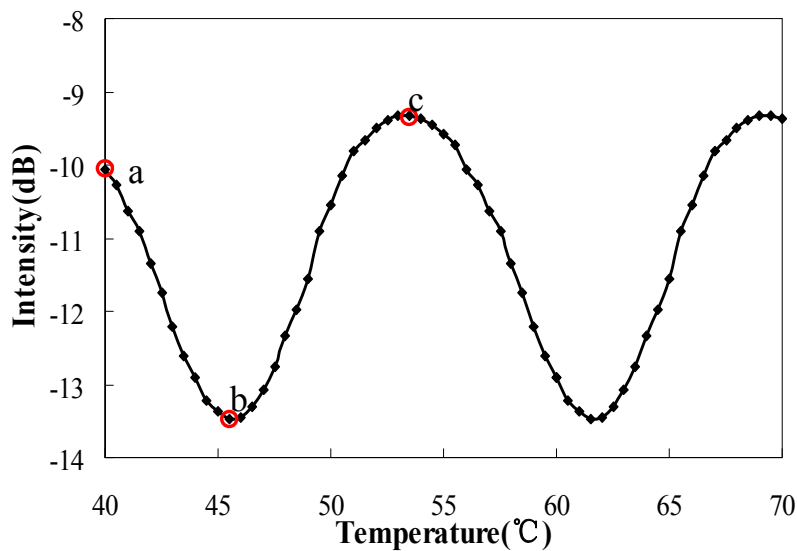


Fig. 26. The relationship of the output power and temperature when the band-pass filter is with a central a wavelength 1545 nm and FWHM 12.66nm.

Fig.27 shows the transmission spectra of the HiBi-FLM, the PCF-LPG, and the output signal without the band-pass filter when temperature is applied at 40 °C, 45.5 °C and 53.5 °C, respectively. The region between the dotted lines is the bandwidth of the band-pass filter. It is clear that the peaks of the FLM shift inside and outside the filter with temperature increasing. Due to the filtering function of the PCF-LPG, the intensity of the output is decided by the location of the FLM's peak in the band of the filter. When the peak is located within a shorter wavelength of the LPG's transmission spectrum, in which a higher transmission is provided, the intensity of the output is larger, as shown in Fig.27 (a) and (c). Obviously, Fig.27 (b) shows the opposite situation. In this case, the peak of the FLM in the filter is near to the transmission dip of the PCF-LPG, thus the intensity of the output is lowest. As shown in Fig.26, the relationship is virtually proportional for temperature from 45.5 °C to 53.5 °C. In this temperature range (8 °C), the intensity change of the output power is 4.137 dB and the change in the transmission wavelength of the FLM is ~6.52 nm which is about half period of the FLM. The fitting function can be written as  $y = 0.0227x^3 + 3.3477x^2 - 163.52x + 2636.6$  with the fitting degree of  $R^2 = 0.9978$ . The average sensitivity of the proposed FLM temperature sensor is about 0.783 dB/°C. When using a power meter with the resolution of 0.01dBm, the temperature resolution is obtained 0.013 °C. The measured temperature range is decided by the wavelength spacing between transmission peaks of the FLM which is given by  $\lambda^2/\Delta nL$ , where  $\lambda$ ,  $\Delta n$ , and  $L$  are the wavelength, the birefringence and the length of the HiBi fiber, respectively. So we can widen the measured temperature range by shortening the length of the FLM. At the same time, a shorter sensor head is convenient in some applications, even though the sensitivity of the sensor will be decreased.

In order to study the effect of the band-pass filter on the sensing performance, several band-pass filters with a center wavelength 1545 nm are used, whose FWHM are 8.3 nm, 6.66 nm and 3 nm, respectively. A serial of experiments are carried out in the same way. Fig.28 shows the relationships of the output intensity and temperature when different filters are used. It is clear that all of them are periodic function and temperature period is 16 °C. The working range of the positive variation region is 8 °C, which is consistent with that of the filter with FWHM 12.66nm. This is because that the wavelength spacing between the transmission peaks of the FLM is not changed all the times. However, they have shown two marked differences: monotone interval and the output intensity range. Table I shows the properties of the proposed FLM temperature sensor when different filters are used.

From Table I, it can be concluded that the average sensitivity of the sensor is higher and the starting temperature of the monotone interval is lower when a filter with a narrower bandwidth is chosen. The reason is that, the transmission peak of the FLM shifts outside the filter band earlier and faster, the monotonicity of the relationship curve will change earlier and the output intensity range will vary larger, and the average sensitivity is also larger because of the same temperature range. When the filter is chosen a FWHM 3 nm with a center wavelength at 1545nm, the average sensitivity of the proposed FLM temperature sensor is about 1.742dB/°C. When a power meter with the resolution of 0.01dBm is used, the temperature resolution is obtained 0.006 °C.

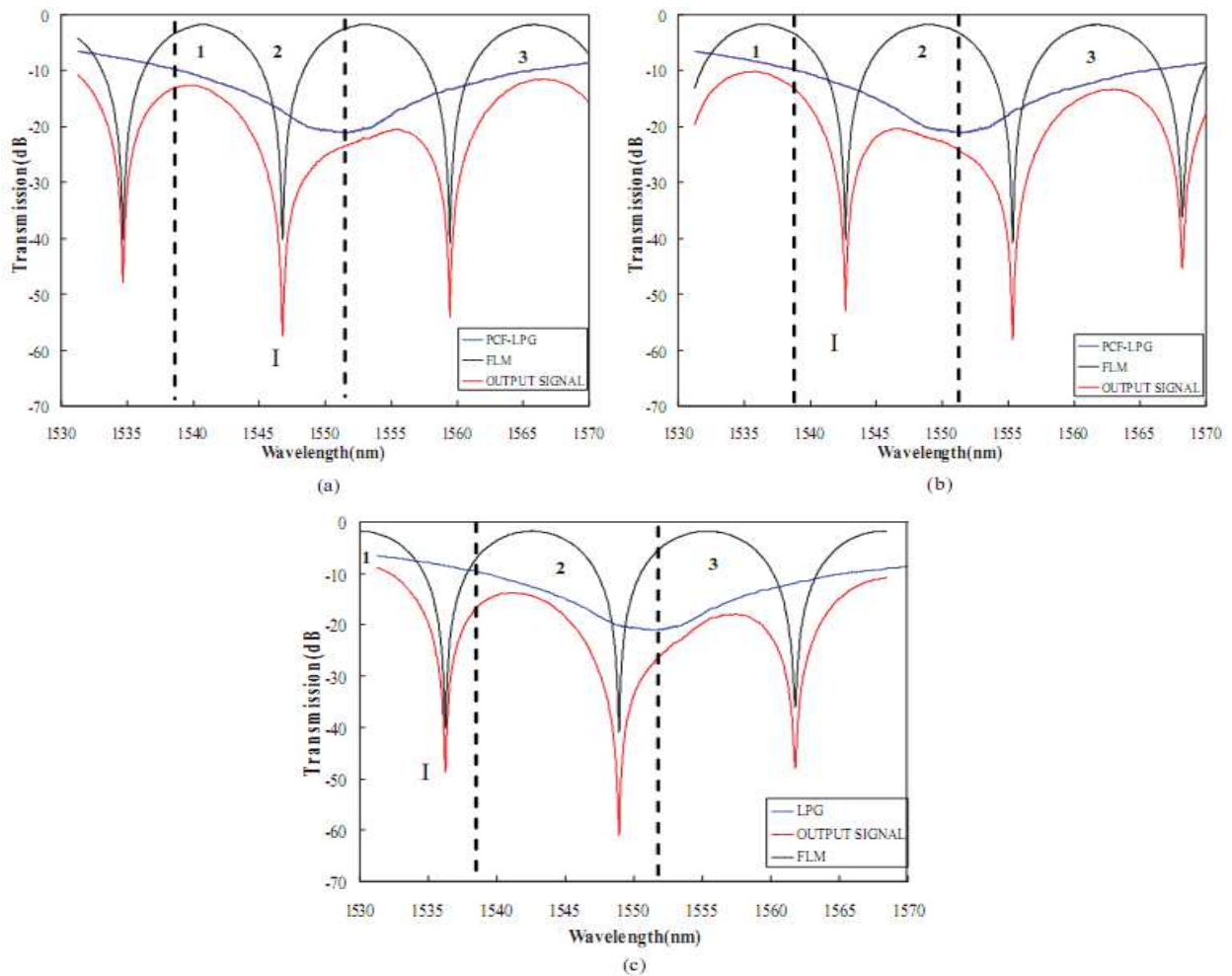


Fig. 27. Transmission spectra of the HiBi-FLM, the PCF-LPG and the output signal when temperature applied on the sensor element is (a) 40°C, (b) 45.5°C, and (c) 53.5°C.

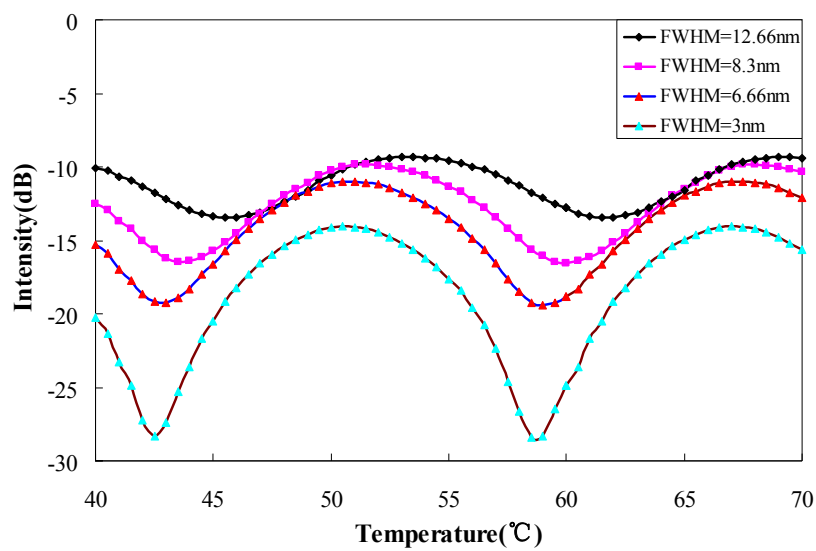


Fig. 28. The relationships of the output power and temperature when different filters are used.

TABLE I. Properties of the proposed FLM temperature sensor when different filters are used.

FWHM	12.66 nm	8.3 nm	6.66 nm	3 nm
Properties				
Monotone interval	45.5 ~ 53.5 °C	43.5 ~ 51.5 °C	43 ~ 51 °C	42.5 ~ 50.5 °C
Output intensity range	-13.4664 dB ~ -9.3291 dB	-16.4375 dB ~ -9.8497 dB	-19.2807 dB ~ -10.9793 dB	-28.3572 dB ~ -14.0612 dB
The fitting function	$y = -0.0227x^3 + 3.3477x^2 - 163.52x + 2636.6$	$y = -0.0249x^3 + 3.5056x^2 - 163.51x + 2509.1$	$y = -0.0188x^3 + 2.5377x^2 - 112.84x + 1632.7$	$y = 0.0068x^3 - 1.2038x^2 + 69.702x - 1337.4$
R <sup>2</sup>	0.9978	0.9988	0.9987	0.9979
Average sensitivity	0.783 dB/°C	1.082 dB/°C	1.222 dB/°C	1.742 dB/°C

Table 1. Properties of the proposed FLM temperature sensor when different filters are used

#### 5.4 Demodulation based on a PCF-LPG with differential processing for a fiber loop mirror temperature sensor [47]

Demodulation systems based on intensity measurement are widely used in optical sensors with simple structures and low costs. However, the sensing accuracy may be decreased since fiber sensor systems often include some noises due to light source fluctuations and all of power fluctuations in the system. In this part, the demodulation based on a PCF-LPG with differential processing for FLM temperature sensor was demonstrated to eliminate the noise of the sensor and raise the sensor accuracy. Utilizing the two linear regions of the transmission spectrum of the PCF-LPG, the variations of the FLM's two resonant wavelengths, which are located respectively within the positive and negative linear region of the LPG's transmission spectrum, are transferred effectively to the intensity variations at the same time. By differential processing of the two signals separated by two band-pass filters, the noise of the sensor is eliminated effectively since the two signals (also including the noise of fiber sensors) transmit through the same path. Experimental results show that the FLM temperature sensor with demodulation based on differential processing of the PCF-LPG is stable.

Fig.29 shows the experimental setup of a HiBi-FLM temperature sensor with the proposed demodulation system based on the PCF-LPG with differential processing. A broadband SLED launches into the HiBi-FLM sensor head. The transmitted light from the HiBi-FLM enters the PCF-LPG, and the output light is split into two beams by a 3 dB coupler, then the two beams enters the signal processing units via two band-pass filters, respectively. The demodulation system is constructed using a PCF-LPG, a 3 dB coupler and two band-pass filters with the full width at half maximum (FWHM) 6.66nm whose center wavelength are 1542nm and 1561.77nm. By utilizing the stable filtering function of the PCF-LPG, the variations of the FLM's resonant wavelengths with temperature, which are located within the positive and negative linear regions of the LPG's transmission spectrum, respectively are transferred effectively to the intensity variations simultaneously. The intensity signals provided by the PCF-LPG are separated effectively by the two band-pass filters whose transmission spectra are shown as the gray regions in Fig. 30. Both signals W1 and W2 are related with the measurand, while they also may include the all of fluctuation of the sensor system. When monitoring W1 or W2, we can obtain the information of temperature applied on the FLM sensor, but the accuracy will be low due to the effect of noises. W1 and W2 are gotten at the same condition since the light from the broadband source passes through the

same path and input to the monitor. By use of the differential processing  $\Delta W = (W1 - W2) / (W1 + W2)$ , the measurement is free from the effect of power fluctuations of the light source and any other noises.

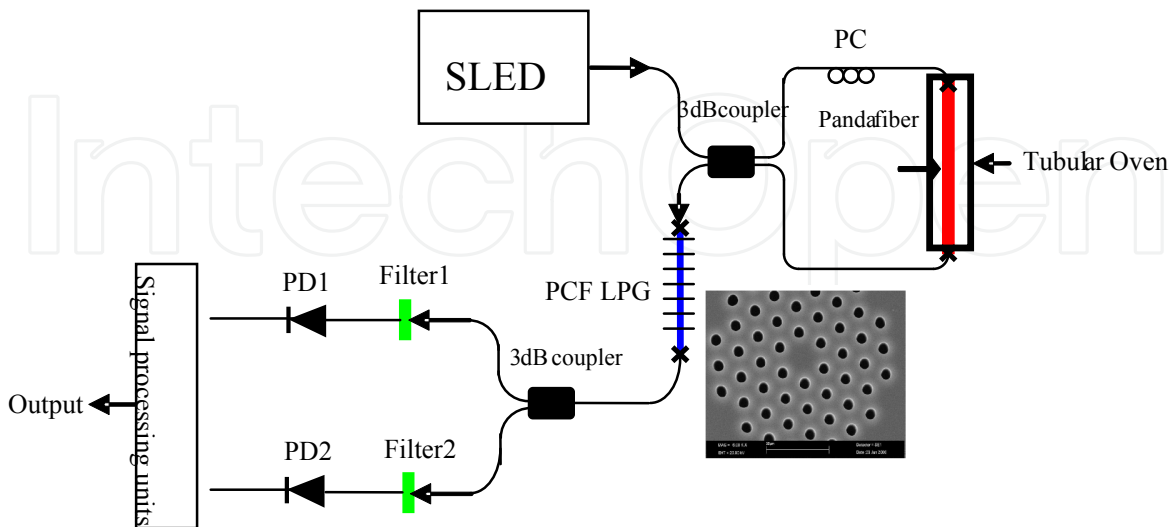


Fig. 29. Experimental setup of the proposed sensor

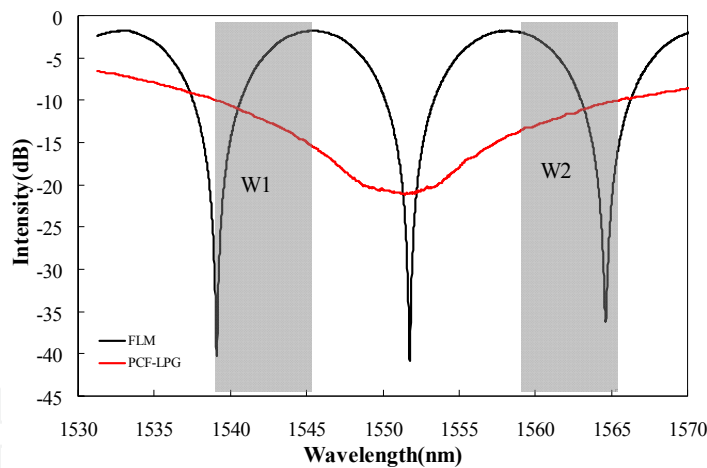


Fig. 30. Transmission spectra of the FLM, the PCF-LPG and the two band-pass filters

Fig.31 shows the relationship of the intensity signal W1 located within a negative linear region of the LPG's transmission spectrum with temperature applied on the FLM. When temperature changes from 47°C to 55°C, the intensity signal W1 will increase with temperature increasing, the sensitivity of the intensity signal W1 to temperature is about 0.01034 mw/°C, and the fitting function can be written as  $Y = 0.0003X^3 - 0.0468X^2 + 2.3668X - 39.652$  with the fitting degree of  $R^2 = 0.9984$ . While the intensity signal W2 will decrease when temperature increasing, the sensitivity of which is about -0.00882 mw/°C, and the fitting function can be written as  $Y = -0.0004X^3 + 0.0572X - 2.8888 + 48.448$  with the fitting degree of  $R^2 = 0.9982$ , as shown in Fig. 32. Fig. 31 and Fig. 32 also show the relationship of the intensity signal W1 and W2 with temperature when the power of the light source



increases 10% and decreases 10%. It is clear that the measurement will deviate from true value and the accuracy of temperature sensor is low.

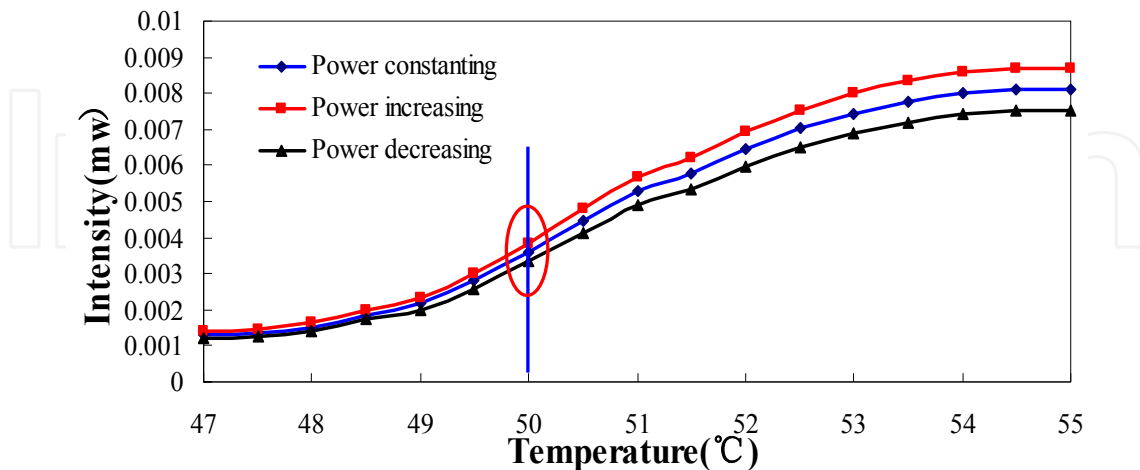


Fig. 31. Relationship of W1 and temperature when the power of light source changes

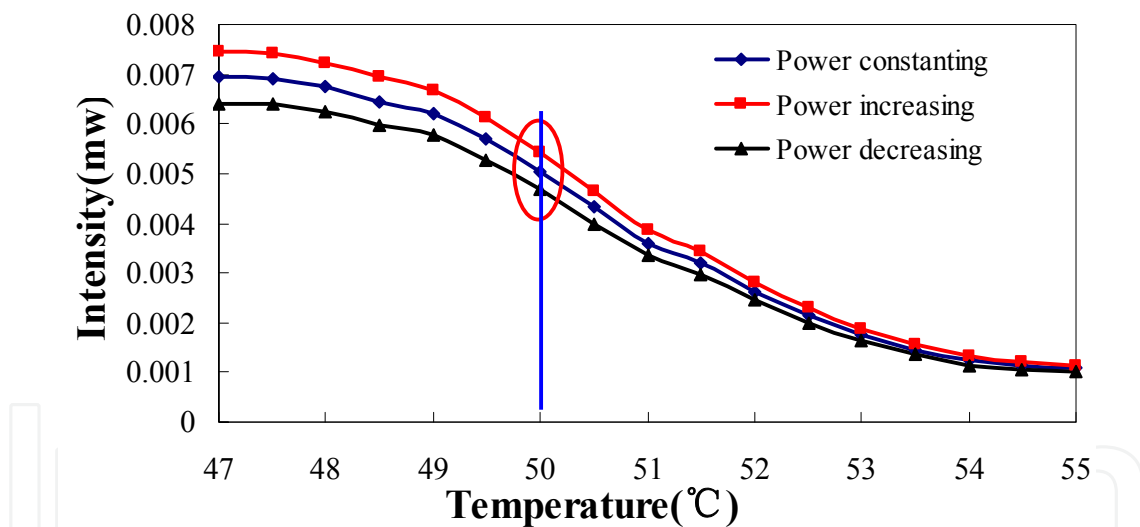


Fig. 32. Relationship of W2 and temperature when the power of light source changes.

Fig.33 shows the relationship of the differential  $\Delta W$  with temperature. The fitting function can be written as  $Y = -0.0075X^3 + 1.138X^2 - 57.382X + 959.39$  with the fitting degree of  $R^2 = 0.9976$  when temperature rises from 47°C to 55°C. When the power of the light source increases 10%, keeps constant and decreases 10%, the relationship of the differential  $\Delta W$  with temperature remains stable and the differential algorithm based on a PCF-LPG eliminates the noises effectively. When the power of the light source changes  $\pm 10\%$ , the measured temperature is 49.83 °C and the relative error is 0.34%. Compared with the result without the differential  $\Delta W$ , the accuracy of the HiBi-FLM sensor rises from  $\sim 90.5\%$  to  $\sim 99.7\%$ .

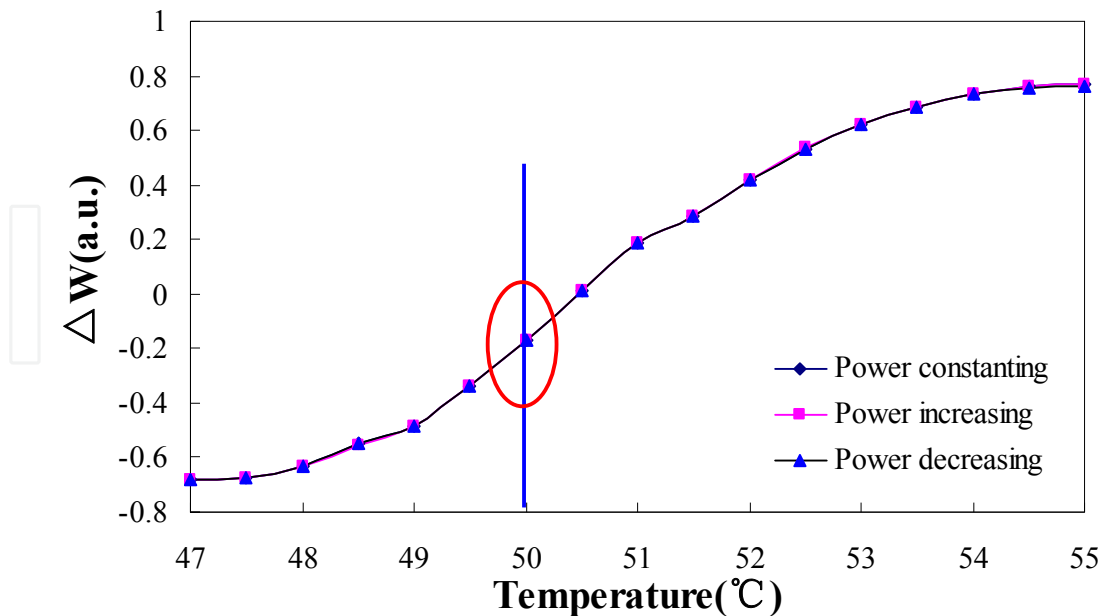


Fig. 33. Relationship of  $\Delta W$  and temperature when the power of light source changes.

## 6. Summary

In this chapter, we have presented the basic operation principle of LPGs, and demonstrated the special properties of PCF-LPGs. By use of a dispersion factor  $\gamma$ , a deeper understanding of the behavior of LPG in the ESM-PCF has been achieved. Both the theoretical and experimental results clearly reveal the significant effect of the waveguide dispersive characteristics of the cladding modes on the strain and temperature characteristics of the LPG in the ESM-PCF. By selecting proper grating period, it is possible to design a LPG with specific strain and temperature properties.

We have shortly reviewed PCF-LPG fabrication methods and mainly described the fabrication method by using a CO<sub>2</sub> laser. The PCF-LPG fabricated under the theoretical design shows a good agreement with the theoretical predictions. Finally, applications of the PCF-LPG in optical fiber sensors have been demonstrated and discussed fully.

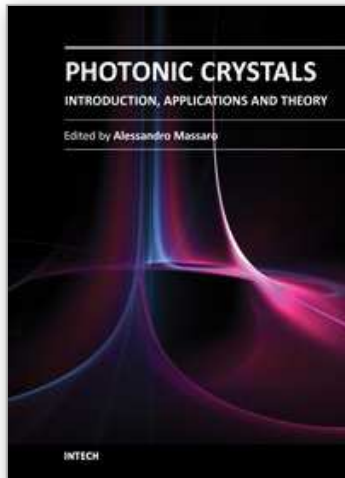
## 7. References

- [1] T. A. Birks, J. C. Knight, and P. St. J. Russell, "endlessly single-mode photonic crystal fiber", *Opt. Lett.* vol. 22, no. 13, pp. 961-963, Jul. 1997.
- [2] J. C. Knight, J. Broeng, and T. A. Birks, "Photonic band gap guidance in optical fibers" *Science*, vol. 282, no. 5393, pp.1476-1478, Nov. 1998.
- [3] J. C. Knight, T. A. Birks, R. F. Cregan, P. St. J. Russell, And J. -P. de Sandro, " Large mode area photonic crystal fiber", *Electon. Lett.* vol. 43, no. 13, pp. 1347, Jul. 1998.
- [4] Ortigosa-Blanch, J. C. Knight, W. J. Wadsworth, J. arriaga, B. J. ManganT. A. Birks, and P. St. J. Russell, "Highly birefringent photonic crystal fibers", *Optics Lett.*, vol. 25, no. 18, pp. 1325-1327, Sep. 2000.

- [5] T. A. Birks, D. Mogilevstev, J. C. Knight, and P. St. J. Russell, "Dispersion compensation using single-material fibers", *IEEE Photo. Technol. Lett.*, vol. 11, no. 6, pp. 674-676, June 1999.
- [6] J. K. Ranka, R. S. Windeler, and A. J. Stentz, "Optical properties of high-delta air silica microstructure optical fibers", *Opt. Lett.* vol. 25, no. 11, pp. 796-798, June 2000.
- [7] J. Ju, W. Jin, M. S. Demokan, "Design of single-polarization single-mode photonic crystal fiber at 1.30 and 1.55  $\mu\text{m}$ ", *J. Lightwave Technol.* vol. 24, no. 2, pp. 825-830, Feb. 2006.
- [8] Charles M. Jewart, Sully Mejía Quintero, Arthur M. B. Braga, and Kevin P. Chen, "Design of a highly-birefringent microstructured photonic crystal fiber for pressure monitoring", *Optics Express*, vol.18, no. 25, pp. 25657, 2010.
- [9] V. Husakou and J. Hermann, "Supercontinuum generation, four-wave mixing, and fission of higher-order solitons in photonic-crystal fibers", *J. Opt. Soc. Am. B*, vol. 19, no. 9, pp. 2171-2182, Sep. 2002.
- [10] J. E. Sharping, M. Fiorentino, A. Coker, P. Kumar, R. S. Windeler, "Four-wave mixing in microstructure fiber", *Opt. Lett.* vol. 26, no. 14, pp. 1048-1050, June 2001.
- [11] W. J. Wadsworth, J. C. Knight, W. H. Reeves, P. St. J. Russell and J. Arriaga, "Yb<sup>3+</sup> - doped photonic crystal fiber laser", *Electron. Lett.* Vol. 36, no. 17, pp. 1452-1454, 2000.
- [12] Z. Yusoff, J. H. Lee, W. Belardi, T. M. Monro, P.C. The, and D. J. Richardson, "Raman effects in a highly nonlinear holey fiber: amplification and modulation", *Opt. Lett.*, vol. 27, no. 6, pp. 424-426, Mar. 2002.
- [13] C.-L. Zhao, Z. Li, X. Yang, C. Lu, W. Jin, M.S. Demokan, "Effect of a nonlinear photonic crystal fiber on the noise characterization of a distributed Raman amplifier", *IEEE Photon. Technol. Lett.*, vol. 17, no. 3, pp. 561-563, Mar. 2005.
- [14] C.-L. Zhao, X. Yang, C. Lu, W. Jin, M.S. Demokan, "Temperature- insensitive interferometer using a highly birefringent photonic crystal fiber loop mirror", *IEEE Photon. Technol. Lett.*, vol. 16, no. 11, pp. 2535-2537, Nov. 2004.
- [15] W. Qian, C.-L. Zhao, S. He, X. Dong, S. Zhang, Z. Zhang, S. Jin, J. Guo and H. Wei, "High-sensitivity temperature sensor based on an alcohol-filled photonic crystal fiber loop mirror", *Opt. Lett.*, vol. 36, pp. 1548-1550, (2011).
- [16] C. Kerbage, R. S. Windeler, B. J. Bggleton, P. Mach, M. Dolinski, and J. A. Rogers, "Tunable devices based on dynamic positioning of micro-fluids in micro-structured optical fiber", *Opt. Commun.*, vol. 204, no. 1-6, pp. 179-184, April 2002.
- [17] W. Qian, C.-L. Zhao, Y. Wang, C. C. Chan, S. Liu, and W. Jin, "Partially liquid-filled hollow-core photonic crystal fiber polarizer", *Opt. Lett.*, vol. 36, no. 16, pp. 3296-3298, 2011.
- [18] Y. L. Hoo, W. Jin, C. Shi, H. L. Ho, D. N. Wang, and S. C. Ruan, "Design and modeling of a photonic crystal fiber gas sensor", *App. Optics*, vol. 42, no. 18, pp. 3509-3515, Sep. 2003.
- [19] N. Burani and J. Lægsgaard, "Perturbative modeling of Bragg-grating-based biosensors in photonic-crystal fibers", *J. Opt. Soc. Am. B*, vol. 22, no. 11, pp. 2487-2493, Nov. 2005.
- [20] M. Vengsarkar, P. J. Lemaire, J. B. Judkins, V. Bhatia, T. Erdogan, and J. E. Sipe, "Long-period fiber gratings as band-rejection filters", *J. Lightwave Technol.*, vol. 14, no. 1, pp. 58-64, Jan. 1996.

- [21] C.-L. Zhao, H.-Y. Tam, B.-O. Guan, X. Dong, P. K. A. Wai, X. Dong, "Optical Automatic Gain Control of EDFA Using Two Oscillating Lasers in a Single Feedback Loop", *Opt. Commun.*, vol. 225, no. 1-3, pp. 157-162, Sep. 2003
- [22] M. Vengsarkar, P. J. Lemaire, G. Jacobovitz-Veselka, V. Bhatia, and J. B. Judkins, "Long-period fiber gratings as gain-flattening and laser stabilizing devices", in *Proc. IOOC'95*, June 1995, PD1-2.
- [23] V. Bhatia and A. M. Vengsarkar, "Optical fiber long-period grating sensor", *Opt. Lett.*, vol. 21, no. 9, pp. 692-694, May 1996.
- [24] V. Bhatia, "Applications of long-period gratings to single and multi-parameter sensing", *Optics Express*, vol. 3, no. 11, pp. 457, May 1999.
- [25] H. J. Patrick, A. D. Kersey, and F. Bucholtz, "Analysis of the response of long period fiber gratings to external index of refraction," *J. Lightwave Technol.*, vol. 16, pp. 1606-1612, Sept. 1998.
- [26] B. J. Eggleton, P. S. Westbrook, R. S. Windeler, S. Spalter, and T. A. Strasser, "Grating resonances in air silica microstructured optical fibers", *Opt. Lett.* vol. 24, no. 21, pp. 1460-1462, Nov. 1999.
- [27] K. Morishita and Y. Miyake, "Fabrication and resonance wavelengths of long-period gratings written in a pure-silica photonic crystal fiber by the glass structure change", *J. Lightwave Technol.*, vol. 22, no. 2, pp. 625-630, Feb. 2004.
- [28] J. Albert, M. Fokine and W. Margulis, "Grating formation in pure silica-core fibers," *Opt. Lett.*, vol. 27, no. 10, pp. 809- 811, May 2002.
- [29] G. Kakarantzas, T. A. Birks, and P. St. J. Russell, "Structural long-period gratings in photonic crystal fibers," *Opt. Lett.*, vol. 27, no. 12, pp.1013-1015, June, 2002.
- [30] Y. Wang, W. Jin, J. Ju, H. Xuan, H. L. Ho, L. Xiao, and D. Wang, "Long period gratings in air-core photonic bandgap fibers", *Optics Express*, vol. 16, no. 4, pp. 2784-2790, 2008.
- [31] H. Dobb, K. Kalli and D.J. Webb, Temperature-insensitive long period grating sensors in photonic crystal fibre, *Electron. Lett.*, vol. 40, no. 11, pp. 657 - 658, May 2004.
- [32] Y. Zhu, P. Shum, H. -W. Bay, M. Yan, J. Hu, J. Hao, and C. Lu, "strain-insensitive and high-temperature long-period gratings inscribed in photonic crystal fiber", *Opt. Lett.*, vol. 30, no. 4, pp. 367-369, Feb. 2005.
- [33] J. H. Lim, K. S. Lee, J. C. Kim, and B. H. Lee, "Tunable fiber gratings fabricated in photonic crystal fiber by use of mechanical pressure", *Opt. Lett.*, vol. 29, no. 4, pp. 331-333, Feb. 2004.
- [34] Diez, T. A. Birks, W. H. Reeves, B. J. Mangan, and P. St. J. Russell, "Excitation of cladding modes in photonic crystal fibers by flexural acoustic waves", *Opt. Lett.* vol. 25, no. 20, pp. 1499, Oct. 2000.
- [35] D.-I Yeom, P. Steinvurzel, B. J. Eggleton, S. D. Lim, and B. Y. Kim, "Tunable acoustic gratings in solid-core photonic bandgap fiber", *Optics Express*, vol. 15, no. 6, pp. 3513-3518, 2007.
- [36] S. Liu, L. Jin, W. Jin, D. Wang, C. Liao, Y. Wang, "Structural long period gratings made by drilling micro-holes in photonic crystal fibers with a femtosecond infrared laser", *Optics Express*, vol. 18, no. 6, pp. 5496-5503, 2010
- [37] L. Jin, W. Jin, J. Ju, and Y. Wang, "Investigation of Long-Period Grating Resonances in Hollow-Core Photonic Bandgap Fibers", *J. Lightwave Technol.* vol. 29, no. 11, pp.1707-1713, 2011.

- [38] C.-L. Zhao, L. Xiao, J. Ju, M.S. Demokan, W. Jin, "Strain and temperature characteristics of a long- period grating written in a photonic crystal fiber and its application as a temperature-insensitive strain sensor", *J. Lightwave Technol.* 26 (2) : 220-227 , 2008.
- [39] K. S. Hong, H. C. Park, and B. Y. Kim, I. K. Hwang, W. Jin and J. Ju, D. I. Yeom, "1000 nm tunable acousto-optic filter based on photonic crystal fiber," *Appl. Phys. Lett.* 92, 031110 (2008).
- [40] Y.-J. Rao, D.-W. Duan, Y.-E. Fan, T. Ke, and M. Xu, "High-Temperature Annealing Behaviors of CO<sub>2</sub> Laser Pulse-Induced Long-Period Fiber Grating in a Photonic Crystal Fiber", *J. Lightwave Technol.*, vol. 28, no.10, pp. 1531-1535, 2010.
- [41] L. Jin, W. Jin, and J. Ju, "Directional Bend Sensing With a CO<sub>2</sub> -Laser-Inscribed Long Period Grating in a Photonic Crystal Fiber", *J. Lightwave Technol.*, vol. 27, no. 21, pp. 4884-4891, 2009
- [42] C.-L. Zhao, J. Zhao, W. Jin, J. Ju, L. Cheng, X. Huang, "Simultaneous Strain and Temperature Measurement Using a Highly Birefringence Fiber loop Mirror and a Long Period Grating Written in a Photonic Crystal Fiber", *Opt. Communications*, 282: 4077-4080, 2009
- [43] Z. He, Y. Zhu, and H. Du, "Long-period gratings inscribed in air- and water-filled photonic crystal fiber for refractometric sensing of aqueous solution", *Appl. Physics Lett.* vol. 92, pp. 044105, 2008.
- [44] Y. Zhu, Z. He, H. Du, "Detection of external refractive index change with high sensitivity using long-period gratings in photonic crystal fiber", *Sensors and Actuators B*, vol. 131, pp. 265-269, 2008.
- [45] C.-L. Zhao, M.S. Demokan, W. Jin, L. Xiao, "A cheap and practical FBG temperature sensor utilizing a long-period grating in a photonic crystal fiber", *Opt. Communications*, 276: 242, 2007
- [46] Y. Wang, C.-L. Zhao, X. Dong, J. Kang, and S. Jin. "A Fiber Loop Mirror Temperature Sensor Demodulation Technique Using a Long-period Grating in a Photonic Crystal Fiber and a Band-pass Filter", *Review of Scientific Instruments*, vol.82, pp.073101, July, 2011.
- [47] Y. Wang, C.-L. Zhao, X. Dong, J. Kang, S. Jin and C. C. Chan. "Demodulation Based on a Long-period Grating in Photonic Crystal Fiber with Differential Processing for High-Birefringence Fiber Loop Mirror Temperature Sensor", *International Conference on Optical Fiber Sensors (OFS)*, Proceedings of SPIE, Vol. 7753, no. 77539c-3, Ottawa, Canada, May 15-19, 2011.
- [48] X. Shu, L. Zhang, and I. Bennion, "Sensitivity characteristics of long-period fiber gratings," *J. Lightw. Technol.*, vol. 20, no. 2, pp. 255-266, Feb. 2002.
- [49] Bertholds and R. Dandliker, "Determination of the individual strain-optic coefficients in single-mode optical fibers," *J. Lightw. Technol.*, vol. 6, no. 1, pp. 17-20, Jan. 1988.
- [50] D.B. Mortimore, "Fiber loop reflectors", *J. Lightwave Technol.* vol. 6, pp. 1217-1224, 1988
- [51] Y. Liu, B. Liu, X. Feng, W. Zhang, G. Zhou, S. Yuan, G. Kai, and X. Dong, "High-birefringence fiber loop mirrors and their applications as sensors," *Appl. Opt.* vol. 44, pp. 2382-2390, 2005



## **Photonic Crystals - Introduction, Applications and Theory**

Edited by Dr. Alessandro Massaro

ISBN 978-953-51-0431-5

Hard cover, 344 pages

**Publisher** InTech

**Published online** 30, March, 2012

**Published in print edition** March, 2012

The first volume of the book concerns the introduction of photonic crystals and applications including design and modeling aspects. Photonic crystals are attractive optical materials for controlling and manipulating the flow of light. In particular, photonic crystals are of great interest for both fundamental and applied research, and the two dimensional ones are beginning to find commercial applications such as optical logic devices, micro electro-mechanical systems (MEMS), sensors. The first commercial products involving two-dimensionally periodic photonic crystals are already available in the form of photonic-crystal fibers, which use a microscale structure to confine light with radically different characteristics compared to conventional optical fiber for applications in nonlinear devices and guiding wavelengths. The goal of the first volume is to provide an overview about the listed issues.

### **How to reference**

In order to correctly reference this scholarly work, feel free to copy and paste the following:

Chun-Liu Zhao (2012). Long-Period Gratings Based on Photonics Crystal Fibers and Their Applications, Photonic Crystals - Introduction, Applications and Theory, Dr. Alessandro Massaro (Ed.), ISBN: 978-953-51-0431-5, InTech, Available from: <http://www.intechopen.com/books/photonic-crystals-introduction-applications-and-theory/long-period-gratings-based-on-photonics-crystal-fibers-and-applications>

**INTECH**  
open science | open minds

### **InTech Europe**

University Campus STeP Ri  
Slavka Krautzeka 83/A  
51000 Rijeka, Croatia  
Phone: +385 (51) 770 447  
Fax: +385 (51) 686 166  
[www.intechopen.com](http://www.intechopen.com)

### **InTech China**

Unit 405, Office Block, Hotel Equatorial Shanghai  
No.65, Yan An Road (West), Shanghai, 200040, China  
中国上海市延安西路65号上海国际贵都大饭店办公楼405单元  
Phone: +86-21-62489820  
Fax: +86-21-62489821

© 2012 The Author(s). Licensee IntechOpen. This is an open access article distributed under the terms of the [Creative Commons Attribution 3.0 License](#), which permits unrestricted use, distribution, and reproduction in any medium, provided the original work is properly cited.

IntechOpen

IntechOpen